communications engineering

Review article

A Nature Portfolio journal

https://doi.org/10.1038/s44172-025-00398-2

Recent progress in hybrid diamond photonics for quantum information processing and sensing

Check for updates

Ryota Katsumi [1,2,3] ✉, Kosuke Takada [2,3], Fedor Jelezko [4] & Takashi Yatsui [2,3]

Point defects in diamond, particularly nitrogen-vacancy (NV) centers, have emerged as powerful tools for a broad range of quantum technologies. These defects are promising candidates for quantum information science, serving as deterministic single-photon sources and solid-state quantum memories. They have also been employed as nanoscale quantum sensors to detect various physical quantities, including magnetic fields, electric fields, and temperature, owing to their long spin coherence time at room temperature. Development of these diamond-based quantum technologies has been rapidly boosted by a recent quantum leap in nanofabrication technologies for high-quality single-crystal diamond. Incorporating these color centers into diamond nanostructures with mature integrated photonics provides a promising route to build scalable and practical systems for quantum applications. This review discusses recent progress and challenges in the hybrid integration of diamond color centers on cutting-edge photonic platforms.

Diamond has been considered a promising material for a wide variety of quantum technologies such as quantum sensing, quantum communication, and quantum computation[1–8]: it can host various types of point defects (nitrogen-vacancy centers (NV), silicon-vacancy centers (SiV), tin-vacancy centers (SnV) and so on) with excellent quantum properties and long spin coherence time. Optically active spin qubits in diamond have shown great potential as solid-state quantum emitters and memories[9], as exemplified by the demonstrations of room-temperature single-photon generation[10] and laboratory-scale quantum network using multiple separate point defects[11]. NV centers are also exploited for sensitive solid-state quantum sensors[12] to detect magnetic field[13–15], electric field[16], strain, and temperature[17,18]. For example, sensing magnetic fields based on a single NV center facilitates the detection of chemical and biomedical information[19–21] and fundamental spin dynamics with atomic scale[22–24]. In addition, the use of an ensemble of NV centers can enhance the magnetic field sensitivities up to the order of picoteslas[15], which is advantageous for medical applications demanding the detection of weak magnetic fields. Solid-state quantum sensors based on diamond are also beneficial for constructing compact and practical devices by combining diamond chips with optical fibers and complementary metal–oxide–semiconductor (CMOS) architectures of silicon photonics.

To unlock the potential of diamond-based quantum technologies, the implementation of micro/nanostructures in diamonds is crucial for the efficient use of NV photons[25–29]. For quantum information processing and quantum sensing, the number of photons in the zero-phonon line (ZPL) and the total number of photons are, respectively, of great importance for practical applications. In quantum information processing, a reduction in coherent photon efficiency leads to errors of computations and low entanglement rates[30–32]. For quantum sensing, the field sensitivity is degraded by a decrease in collected amount of NV photons[3]. Owing to recent advancements in diamond nanofabrication technologies, a wide variety of nanophotonic structures have been successfully demonstrated to date[33]. However, the scalability is limited by the lack of the technology to fabricate wafer-scale diamond photonic integrated circuits. Also, diamond photonics is not fully developed in terms of quality, functionality, and compatibility with electronics compared to well-developed photonic platforms, including Si, SiN, $LiNbO_3$ and AlN. The attractive and alternative approach is the hybrid integration of diamond color centers on these sophisticated photonic platforms[34–36]. For instance, Si photonics will be a key enabling technology to build large-scale and highly functional photonic circuits[37,38] owing to mature CMOS technology. SiN photonics is also compatible with CMOS fabrication[39] and offers ultra-low photonic loss[40,41]. Meanwhile, the current nanofabrication technology for diamond photonics is inherently incompatible with existing hybrid integration approaches. Thus, the open question is how to combine diamond photonics with other state-of-the-art photonic technologies for future scalable and functionalized quantum applications.

[1]Department of Electrical Engineering, Columbia University, New York, New York, NY, USA. [2]Graduate School of Engineering, Toyohashi University of Technology, Toyohashi, Aichi, Japan. [3]Graduate School of Engineering, the University of Tokyo, Bunkyo-ku, Tokyo, Japan. [4]Institute of Quantum Optics, Ulm University, Ulm, Germany. ✉e-mail: rk3339@columbia.edu

This contribution reviews the hybrid integration of diamond color centers into cutting-edge photonics platforms. We first provide a brief overview of NV's creation and diamond etching technology. We then summarize the advances in hybrid integration of diamond on a photonic chip for quantum information processing and quantum sensing. Moreover, we also discuss the related technologies including cryo-CMOS and compact diamond quantum sensors. We then discuss the future challenges and opportunities of diamond quantum photonics with heterogeneous photonics chips.

Creation of color centers in diamond

This section briefly introduces color centers in diamond and the ways to create them.

Color centers in diamond

NV centers and group-IV color centers in diamond exhibit different structural symmetries. These differences result in distinct spin properties and influence their applications in quantum technologies. Detailed information regarding the physics of color centers in diamond is provided in these articles[42–45]. An NV center is created when a nitrogen atom replaces a carbon atom in the diamond lattice adjacent to a lattice vacancy, resulting in C_{3v} symmetry (Fig. 1a). Thanks to their high radiative quantum efficiency even at room temperature, as well as the short decay time of their excited state, NV centers can operate as excellent solid-state single-photon emitters (Fig. 1b)[10,46]. In addition, the efficient spin-photon interface of NV centers makes them well-suited as nodes in a long-distance quantum network[47–51]. Recent work has successfully demonstrated three-node entanglement-based quantum network that consists of three spatially independent quantum nodes based on NV centers, labeled Alice, Bob, and Charlie (Fig. 1c)[7]. Through the development of phase and frequency stabilization, they have demonstrated two quantum network protocols without postselection: the distribution of genuine multipartite Greenberger-Horne-Zeilinger (GHZ) entangled states across the three nodes and entanglement swapping via an intermediary quantum node. Its long spin coherence is also advantageous to build a quantum memory. By combining dynamical decoupling of an electron spin with selective phase-controlled driving of nuclear spins, a ten-qubit quantum register consisting of the electron spin of an NV center and nine nuclear spins in diamond has been demonstrated (Fig. 1d)[52]. The protection of an arbitrary single-qubit state has been demonstrated for over 75 s—the longest reported for a single solid-state qubit—and two-qubit entanglement has been preserved for over 10 s.

NV center is also considered as a leading candidate for a quantum sensor that are able to accurately detect various physical quantities including magnetic field, temperature, strain, and electric fields[4]. In particular, it has shown considerable promise as a magnetometer for a wide range of applications, owing to its long spin coherence time. The principle of magnetic sensing relies on the energy level structure of the electrons, as illustrated in Fig. 2a. The electron energy of the NV^- center can be controlled by a green laser (typically 532 nm) and microwave irradiation. When the spin state $m_s = 0$ transitions to $m_s = \pm1$ via microwave irradiation, the red fluorescence intensity decreases due to the population transfer to the non-radiative singlet state. Figure 2b shows an optically detected magnetic resonance (ODMR) spectrum, where optical and microwave methods are combined to probe the spin states of defects, such as NV centers, through changes in fluorescence intensity. Under an external magnetic field, the energy level of $m_s = \pm1$ splits owing to the Zeeman effect, resulting in splitting the dip in Fig. 2b. This sensitive shift in dips caused by subtle changes in the magnetic field enables NV centers to function as highly sensitive magnetometers. Moreover, NV's long spin coherence time—even at room temperature—makes it an ideal platform for quantum sensing devices, in contrast to other quantum sensor technologies such as superconducting quantum interference devices (SQUIDs) and optically pumped magnetometers (OPMs).When single NV center is embedded in the edge of a diamond scanning probe[53] or diamond nanobeam[54], this serves as an atomic-scale quantum sensor to explore condensed matter physics. For instance, probe-based sensing has been employed for studying atomically thin crystals of the 2D van der Waals magnets (Fig. 2c)[55,56]. The nanobeam-based approach has been utilized for exploring the property of magnons (Fig. 2d)[23,57]. Applications of NV centers for condensed matter physics is deeply discussed in ref. 22. When NV centers are shallowly implanted in diamonds, they can function as magnetic resonance imaging (MRI, Fig. 2e)[58] and nuclear magnetic resonance (NMR, Fig. 2f)[59] at nanoscale for proteins, molecules, and DNA (see also ref. 21).

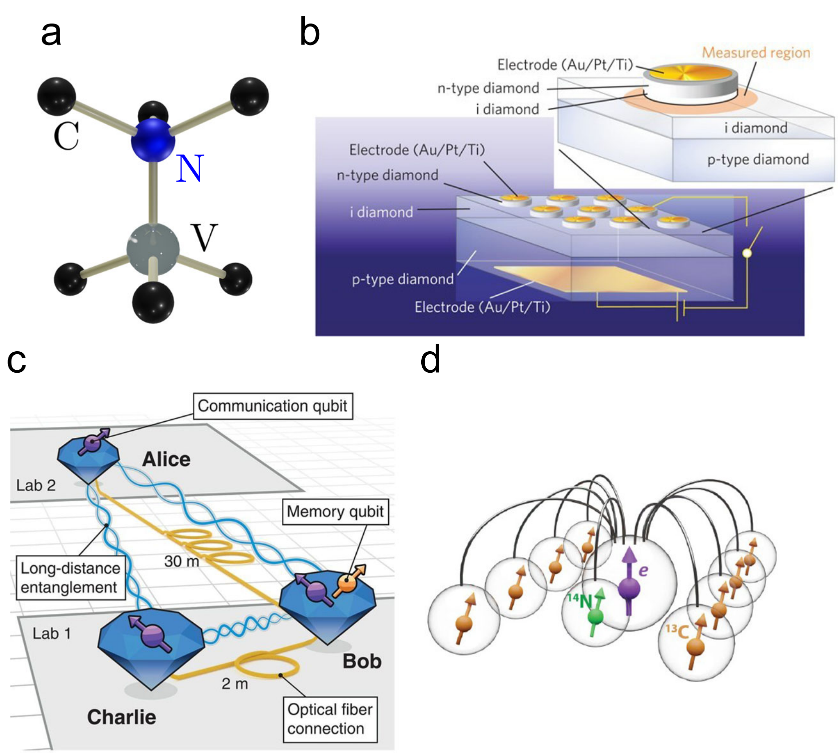

Fig. 1 | Quantum technologies based on NV centers in diamond. **a** Crystal structure of an nitrogen-vacancy (NV) center, showing C_{3v} symmetry. **b** Single photon source based on NV centers located in the i-layer of p-i-n junction to be electrically driven. Reproduced with permission from Springer Nature. Copyright 2012[10]. **c** Entanglement generation among remote NV centers, mediated by the polarization states of flying photons. Reproduced with permission from AAAS. Copyright 2021[11]. **d** Quantum register constructed from ten qubits: electron and nuclear spins of NV center and surrounding eight nuclear spins of ^{13}C isotope. Reproduced from ref. 52 under the terms of the Creative Commons Attribution License (CC BY 4.0).

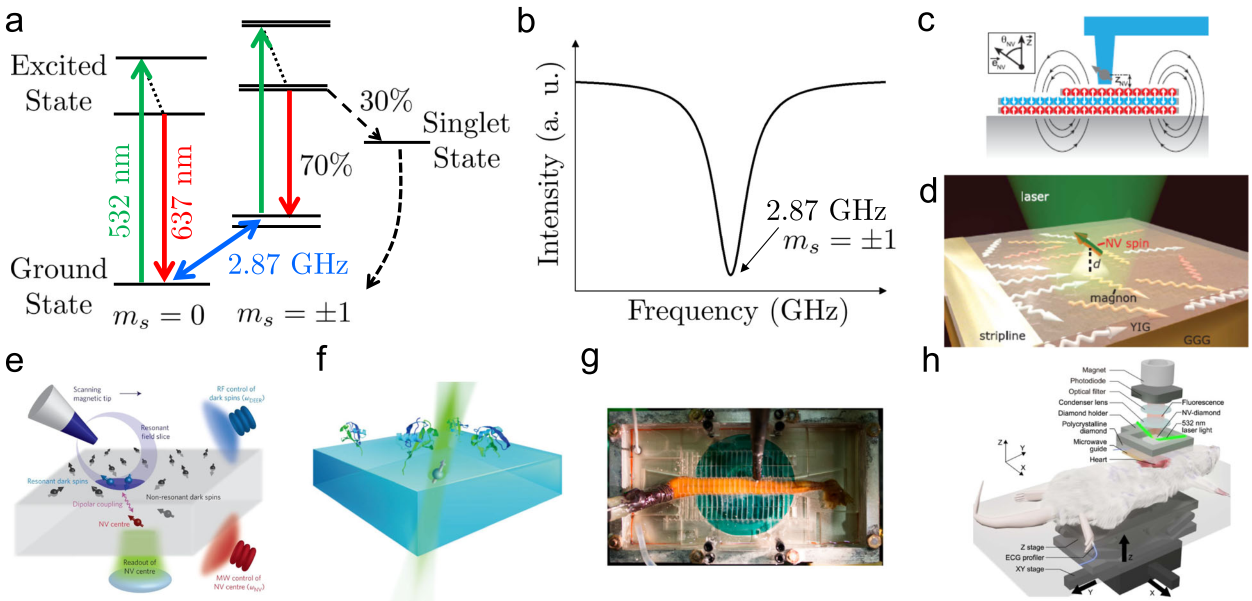

Fig. 2 | NV centers for quantum sensing applications. **a** Optically ground and excited energy levels of the triplet electron spin in the NV center. Spin-selective decay via the singlet states occurs when the system is optically pumped, leading to the decreased red fluorescence intensity for magnetic-field-sensitive $m_s = \pm1$ states. **b** Zero-bias optically detected magnetic resonance (ODMR) spectrum of the NV center as a response to optical pumping and frequency-swept microwave irradiation. **c** Diamond scanning probe equipped with the single NV center for detecting magnetic fields produced by 2D van der Waals magnets. Reproduced with permission from AAAS. Copyright 2019[55]. **d** Detection of magnons using the NV center embedded in a diamond nanobeam structure. Reproduced with permission from AAAS. Copyright 2021[57]. **e** Subnanometer-scale MRI setup enabled by a shallowly implanted single NV center. Reproduced with permission from Springer Nature. Copyright 2014[58]. **f** NMR-based detection of protein molecules using a shallow single NV center. Reproduced with permission from AAAS. Copyright 2016[59]. **g** Noninvasive detection of neuron activity in a living marine worm via magnetometry using an ensemble of NV centers. Reproduced with permission from ref. 67. **h** Magnetocardiography using the bulk diamond chip containing an ensemble of NV centers as a millimeter-scale sensor. Reproduced from ref. 69 under the terms of the Creative Commons Attribution License (CC BY 4.0).

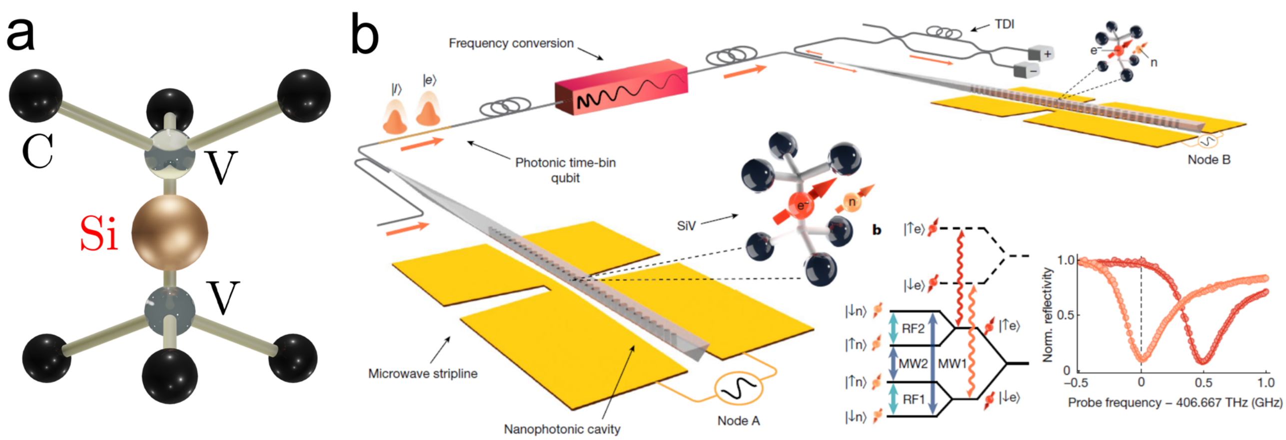

Fig. 3 | SiV centers in diamond for quantum information technologies. **a** Crystal structure of a silicon-vacancy (SiV) center, showing D_{3d} symmetry. **b** Remote entanglement generation between the SiV centers embedded in photonic crystal cavity systems, mediated by time-bin photon states and the efficient spin-photon interface. Reproduced from ref. 73 under the terms of the Creative Commons Attribution License (CC BY 4.0).

Robust nature of diamond also allows us to explore condensed matter physics at megabar pressures[60–62]. Moreover, magnetic field sensitivities of the order of picoteslas have been achieved by employing an ensemble of NV centers (with a typical density of $\sim10^{17}$ cm^{-3})[15,63], which is beneficial for biological and medical applications that involve detecting weak magnetic fields. To date, the best field sensitivity is reported to be 210 $fT/\sqrt{Hz}$ (0.5 $nT/\sqrt{Hz}$) using ensemble NV centers[63] (a single NV center[64]). Recent studies have demonstrated the magnetic imaging of living cells at nanoscale[65,66], magnetic detection of action potentials in living large squid (Fig. 2g)[67] and muscle fibres[68], and magnetocardiography of living rats at a millimeter-scale (Fig. 2h)[69]. Furthermore, NV centers in diamonds are also being studied for other fascinating applications, including the development of gyroscope[70] and investigation of geological samples[71].

For group-IV color centers, the group-IV atom is located at an interstitial lattice site between two vacancies of diamonds. Surprisingly, Debye–Waller factor (i.e., the fraction of radiative emission occurring within the ZPL) is 70% for SiV centers, significantly higher than that of NV centers (~3%) and thus suitable for quantum communications and quantum photonic computing. The inversion-symmetric D_{3d} structure of the defect (Fig. 3a) also results in no permanent electric dipole, making the optical transition insensitive to electric field fluctuations and thereby protecting the optical coherence. Recent work has demonstrated a two-node quantum network composed of multi-qubit registers based on SiV centers in diamond nanocavities[72], which has been further integrated with a telecommunication fiber network and periodically-poled lithium niobate devices in a more recent study (Fig. 3b)[73]. Each SiV is localized in a nanophotonic cavity within an individually operated cryostat held at temperatures below 200 mK in two separate laboratories. Long-lived nuclear spin qubits are employed to provide second-long entanglement storage and integrated error detection. By integrating efficient bidirectional quantum frequency conversion of photonic communication qubits from visible (737 nm) to telecom wavelength (1350 nm), the entanglement of two nuclear spin memories has been achieved through 40 km spools of low-loss fiber and a 35-km long fiber loop deployed in the Boston area urban environment. However, one of the drawbacks of SiV centers is the operation temperature (below 1 K). To this end, other group-IV vacancies operating at higher temperature, such as SnV[74,75] and lead vacancy (PbV) centers[76,77] are being intensively studied recently (see also ref. 43).

Ion implantation

The most common way to create color centers in diamond is ion implantation: accelerating ions (e.g., nitrogen and silicon) of an element into diamond. In this process, vacancies are introduced at the same time and subsequent annealing creates defect centers. This method enables us to control the depth of defect centers from the top surface, which can be calculated via stopping and range of ions in matter (SRIM) simulations. To create defects in the middle of diamond nanostructures (close to the diamond surface) for single photon sources (quantum sensors), the nitrogen ions are typically implemented into a pure single-crystal diamond (i.e., a type-IIa diamond) with energies of ~100 (6) keV, which results in mean implantation depths of ~110 (10) nm[78]. The subsequent annealing procedure activates the migration of vacancies to implanted nitrogen impurities, leading to the formation of NV defects. We note that single NV center close to the diamond surface serves as a sensitive and atomic-scale quantum sensor for a broad spectrum of research field ranging from chemistry, biology[19–21] and condensed matter physics[22–24]

The advantage of this approach is that we can precisely control the position of point defects when combined by mask structure. For instance, NV center was created at the center of a photonic crystal cavity by combining nitrogen ion implantation and silicon masks, resulting in the horizontal positional accuracy of 50 nm which is limited by the aperture size of the mask[79]. Another promising approach is based on a focused ion beam, which can create single color center without mask structures[80–83]. For both approaches, the horizontal positional derivation (i.e., the depth spread due to implantation) is better than 30 nm. Meanwhile, these approaches have a relatively low yield; the reported yield for creating NV (SiV) centers using ion implantation (focused ion beam) is approximately 25%[79] (20%)[82].

Electron irradiation

An ensemble of NV centers is powerful to enhance the sensitivity of quantum sensing. Ensembles of NV centers in diamond can be produced through electron irradiation. Starting from a diamond sample with a high density of nitrogen impurities (i.e., a type-Ib diamond), NV defects can be efficiently created through high energy irradiation of electrons and subsequent annealing of the sample. The concentration of NV centers is 1.8 ppm ($3.2 \times 10^{17}\,\mathrm{cm}^{-3}$) with a total fluence of 5×10^{17} electrons cm^{-2} and an irradiation power of 2.0 MeV[69]. We note that there is a trade-off between the spin coherence time and the NV density, since the nearby unconverted nitrogen and created NV centers are dominant sources of decoherence. More detailed discussion can be found the following ref. 3.

Laser writing

Laser processing was shown to be an effective approach to introduce color centers in diamond. This approach induces vacancies into diamonds without residual damage, allowing us to bind with existing substitutional nitrogen impurities in the lattice to create high-quality single NV centers[84,85]. Recently, by employing femtosecond laser processing to not only create vacancies in the crystal but also anneal the diamond, the creation of NV centers with in-plane position derivation of ~30 nm and near-unity yield (96%) has been demonstrated[86]. However, this approach suffers from the relatively poor depth positioning accuracy of the resultant NV centers which was limited to a few hundred nanometers. This would be improved by using delta doping of nitrogen impurities[87–91], where a thin nitrogen-doped layer is formed by adding nitrogen gas during the diamond growth process. This approach can create a slab of shallow NV within a depth precision of few nanometers.

Breakthrough in diamond nanotechnology

To accelerate advances in diamond-based quantum technologies, it is important to implement micro/nanostructures in diamonds. However, the heteroepitaxial growth of high-quality single-crystal diamond thin films on different materials is challenging due to the current diamond growth technology[92]. Therefore, in this section, we will summarize the advances since the 2010s in the nanofabrication based on single-crystal diamond. The growth of single-crystal diamonds are introduced elsewhere[93].

Thin-film fabrication based on etching

It is desirable to prepare diamond thin films on other substrates, following silicon-on-insulator platforms. To this end, a thinning-membrane approach was proposed. In 2011, a 280-nm-thick diamond membrane was fabricated on silicon oxide by thinning a 5-μm-thick type IIa single-crystal diamond membrane[94]. During the diamond plate thinning by using oxygen plasma, the membrane was mounted on a 2 mm-thick SiO_2 substrate thermally grown on a silicon wafer (Fig. 4). By following the standard nanofabrication procedure, a ring resonator with a Q-factor of ~4000 was reported. Up to now, various photonic structures were demonstrated based on this approach, including a waveguide-coupled ring resonator[95–98], one dimensional PhC[99,100], and two dimensional PhC[101,102]. The negative aspect of this approach, however, is the non-uniform thickness of the membrane (so-called "wedging") due to non-uniform thickness of the starting, mechanically polished material, which hinders scalable fabrication of diamond PhC cavities.

Angled etching

Another nanofabrication approach is based on "angled etching", which can fabricate suspended nanobeam structures with triangular cross-sectional profile by applying ions of oxygen plasma to diamond at an oblique angle (Fig. 5a). The first demonstration of angled etching for diamond was performed by placing a single-crystal diamond chip in a perforated metal structure designed for use in conjunction with an inductively coupled plasma reactive ion etching (ICP-RIE) (so-called "Faraday cage")[103]. The trajectories of ions were modified by the Faraday cage in the chamber, resulting in the undercut of nanostructures in single-crystal diamond with triangular cross sections. Since then, this approach has been employed to fabricate a wide variety of structures such as racetrack resonators (Fig. 5b)[104], one-dimensional PhC nanobeams[79,104], nanocone structures[105], and photonic wire waveguide[106–108]. It is notable that angled etching has also been utilized to fabricate nanostructures in other single-crystal materials such as silicon carbide[109,110], quartz[111], and gallium nitride[112].

However, photonic devices fabricated with Faraday cage exhibit non-uniformity across the substrate due to position-dependent variations in ion trajectories[113,114]. An alternative approach for reproducibility is reactive ion beam angled etching (RIBAE)[115]. In this method, the ion beam generated in an ion gun is collimated and accelerated towards the chamber through a series of grids. The ion beam can be made uniform over an area of diameter as large as 4-inch, enabling improved undercut etch uniformity over the entire area of a bulk diamond substrate when tilting the sample stage. RIBAE has been used to fabricate photonic devices including diamond mirrors for high power laser[116], dispersion engineered waveguides for supercontinuum generation[108], and one-dimensional PhC cavities for quantum network[73,117,118]. Nevertheless, the drawback of angle etching is that achievable nanostructures are limited: angled etching is not compatible with

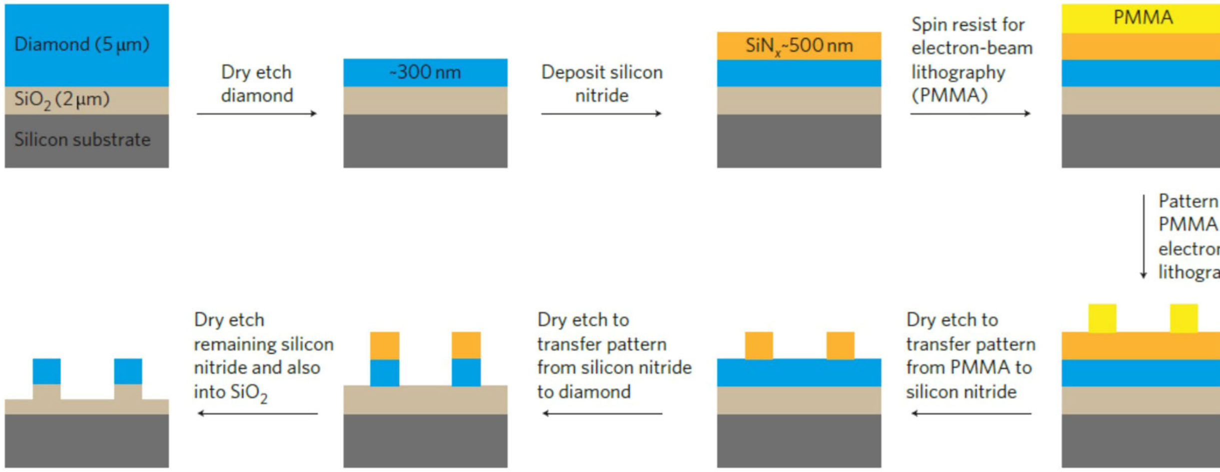

Fig. 4 | Top-down dry etching process of diamond via thinning-membrane approach. The thick diamond plate is dry etched down to a few hundreds of nm thickness, followed by mask and resist layer deposition and lithography. Reproduced with permission from Springer Nature. Copyright 2011[94].

Fig. 5 | Detailed description of angled etching. **a** Angled-etching procedure following: (i) mask formation, (ii) vertical etching of diamond, (iii) angled etching via anisotropic plasma injection with an oblique angle, (iv) removal of the mask. Adapted with permission from ref. 103. Copyright 2012 American Chemical Society. **b** Racetrack resonator as an example of the angled-etched diamond structure. Reproduced with permission from Springer Nature. Copyright 2014[104].

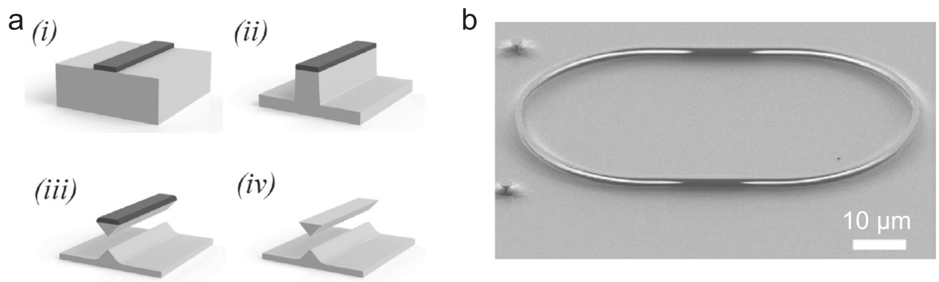

the fabrication of specific waveguide structures and two-dimensional PhCs because of the resulting characteristic triangular cross-sectional profile.

Quasi-isotropic etching

Alternative and fascinating approach to produce air-suspended photonic structures is "quasi-isotropic etching". This technique relies on a zero bias oxygen plasma after standard vertical RIE. Figure 6a illustrates the procedure of the quasi-isotropic etching[119]. (i) First, polished bulk single crystal diamond chips are cleaned in boiling piranha and coated with thick hard mask (e.g., silicon nitride based on PECVD or LPCVD). The samples are then coated with an electron beam resist (e.g., ZEP 520 A and HSQ). (ii) Nanostructures are patterned in the resist by performing electron beam lithography and subsequent development. (iii) Patterns are transferred to the hard mask by standard dry etching. (iv) Patterns are transferred to the diamond by anisotropic oxygen-plasma-based ICPRIE etching. (v) The sidewalls of etched diamond are protected with a conformal layer deposited by atomic layer deposition of aluminum oxide or PECVD of silicon nitride. (vi) A short ICPRIE etch removes top protective layer, leaving only the sides covered. (vii) A zero-bias oxygen ICPRIE plasma undercuts the nanostructures. The elevated temperature and pressure enhance the etch rate of diamond. (viii) The sample is soaked in HF to remove the remaining hard mask and protective layer. Figure 6b, c display the SEM images of disk resonator[119] and one-dimensional PhC[120] fabricated by quasi-isotropic etching, respectively. To date, nanostructures such as disk resonators[119,121], photonic waveguides[122], one-dimensional PhC nanobeams[123–126], phononic crystal[127], two-dimensional PhC cavities[128], and nanobeam quantum sensor[24] have been successfully fabricated by using the quasi-isotropic etching. Nevertheless, the relatively complicated etching procedure causes fabrication imperfections such as rough side walls of etched surfaces and non-flat bottom surface, which results in the experimentally limited Q factors $< \sim 10^4$ at visible wavelength.

Smart cut approach

Both angled and quasi-isotropic etching are the most common approaches in diamond nanophotonics to date. However, they generally suffer from several challenges as discussed above. In addition, typical Q factors of the nanocavities demonstrated by these methods ($\sim 10^4$) are much lower than those simulated ($\sim 10^6$) due to fabrication imperfections stemming from complicated etching procedures. An ion slicing (or so called "smart cut") technique is promising to produce large-area and uniform thin membrane from single-crystal diamond for high-quality diamond nanophotonics. Smart cut technique is based on ion implantation, which creates a graphitized layer near the top surface of diamond that can be easily removed by electrochemically etching. Historically, the proof-of-concept demonstration for ion slicing was experimentally shown in 1992[129]. Since then, several groups demonstrated the fabrication of nanostructures by using the diamond membrane ion-sliced based on H^+ or He^+ ion[130–132]. However, the critical issues were the ion damage in these films and residual built-in strain induced by ion implantation[133]. Recently, X. Guo et al. proposed the novel approach of fabricating high-quality diamond membrane by combining smart-cut technique with subsequent regrowth of diamond layer[134,135]. Figure 7a shows the basic flow of preparing high-quality diamond thin membranes. First, He^+ implantation with subsequent annealing is preformed to form the graphitized layer (dark gray underneath the top diamond membrane). Color centers are created via either ion implantation. Diamond membrane is undercut through electrochemical etching in DI water. Next, the air-suspended membrane is transferred to another substrate by utilizing transfer printing. Finally, the damaged layer is removed by

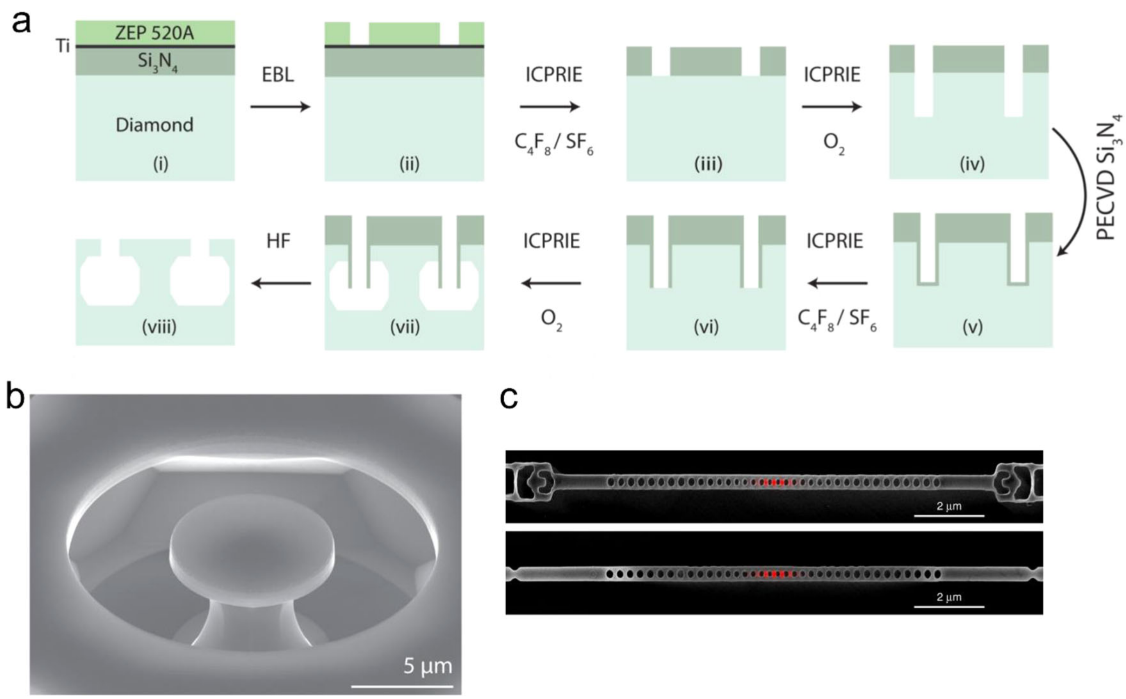

Fig. 6 | Quasi-isotropic etching. a Fabrication steps: (i) resist deposition, (ii) resist patterning, (iii) mask patterning, (iv) vertical etching, (v) mask layer deposition on side walls, (vi) selective removal of bottom masks, (vii) undercut by zero-bias oxygen plasma etching, and (viii) removal of whole masks. **b** Scanning microscope image (SEM) of a disk resonator fabricated by quasi-isotropic etching. Adapted with permission from ref. 119. Copyright 2015 American Chemical Society. **c** Photonic crystal structure as another example. EBL electron beam lithography, ICPRIE inductively coupled plasma reactive ion etching, PECVD plasma-enhanced chemical vapor deposition. Reproduced from ref. 120 under the terms of the Creative Commons Attribution License (CC BY 4.0).

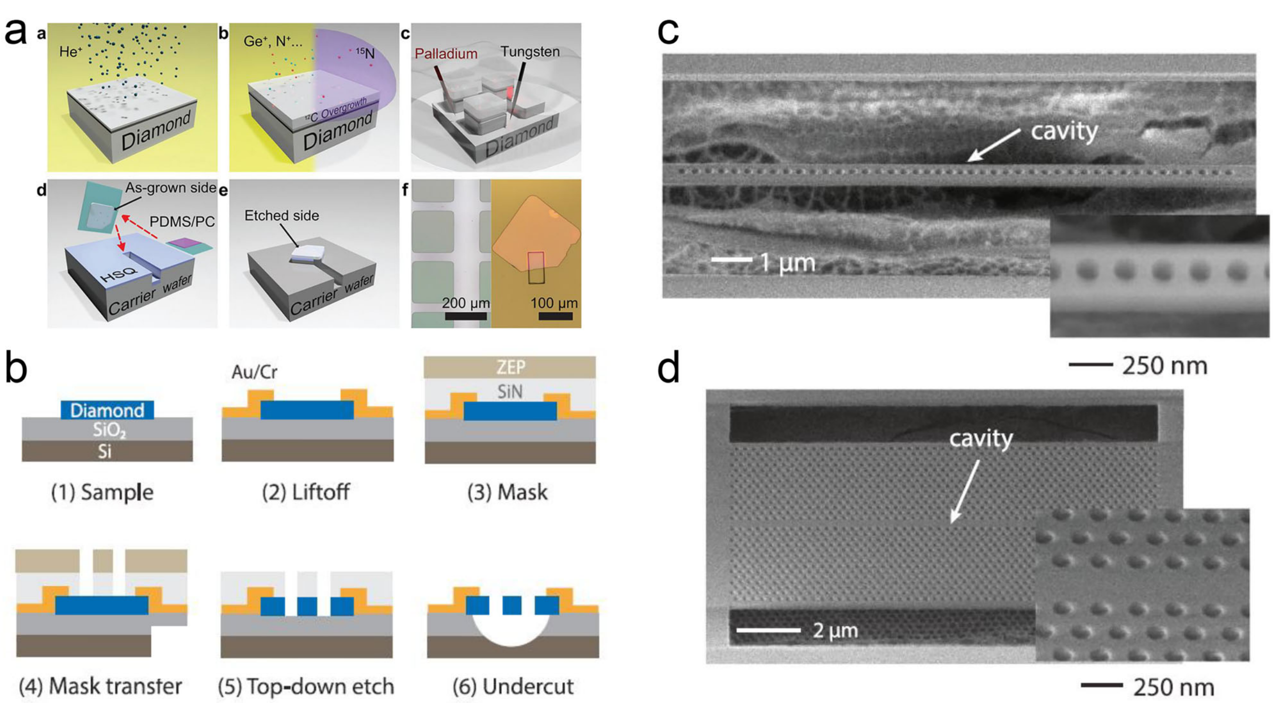

Fig. 7 | Diamond nanofabrication based on smart cut approach. a Membrane fabrication process via graphitized layer formation, crystal overgrowth with optional ion implantations, electrochemical etching, flip and transfer of the suspended membrane, and removal of the damaged layer by the dry etching stopped at the regrown layer. Reproduced from ref. 134 under the terms of the Creative Commons Attribution License (CC BY 4.0). **b** Description of fabrication process, including: (1) initial condition of a sample, in which a diamond membrane is placed on top of a SiO_2 substrate, (2) formation of metal frame via liftoff process, (3) deposition of mask and resist layer, (4) transferring of lithography pattern to the mask layer, (5) top-down etching of the diamond membrane along the mask, and (6) undercut by wet etching process. **c** One-dimensional and **d** two-dimensional photonic crystal cavities with inversion symmetry against height direction to achieve high quality factor, enabled by the undercut. Reproduced from ref. 136 under the terms of the Creative Commons Attribution-NonCommercial-NoDerivatives License (CC BY-NC-ND 4.0).

oxygen-based dry etching. By leveraging this high-quality diamond membrane, S. Ding et al. demonstrated one- and two-dimensional diamond PhC cavities with Q factors of 1.8×10^5 and 1.6×10^5, respectively[136]. Figure 7b shows the process flow of the diamond nanofabrication, which is very similar to the standard semiconductor process. Figure 7c, d display the SEM images of one- and two-dimensional diamond PhC cavities based on the smart cut approach. We note that Q-factors demonstrated by their group are the highest for visible PhC cavities of any material. This technology will be expected to establish a new paradigm in diamond nanophotonics. This approach may face challenges such as poor adhesion and strain of diamond membranes during the hybrid integration on chip. We consider that chemical surface treatment and post-annealing could effectively enhance adhesion and relieve strain[137,138]. It is also noteworthy that thin-film diamond membranes based on the smart-cut approach or oxygen plasma etching present significant challenges for scalable production due to their time-consuming and scale-limited processes. A promising solution to address this issue is inspired by the mechanical exfoliation method for thin-film polycrystalline diamond membranes[139,140]. A recent study demonstrated that edge-exposed exfoliation using adhesive tape enables mass production of large-area (2-inch wafer), ultrathin (sub-micrometer thickness), ultraflat (sub-nanometer surface roughness), ultraflexible (360° bendable), and transferrable diamond membranes[141].

The proposed membrane approach is also highly compatible with a miniaturized Fabry-Pérot microcavity, which is based on an optical fiber and a mirror and has been employed for various quantum emitters including semiconductor quantum dots[142,143], point defects in diamond[144,145] and 2D materials[146,147], and organic molecules[148]. This type of cavity offers the advantage of in situ spatial and spectral tuning, combined with high Q-factors and excellent mode matching to a propagating Gaussian beam, albeit at the cost of a large mode volume (typically $\sim 125 \times \left(\frac{\lambda}{n}\right)^3$). This approach has enabled Purcell enhancement and precise position control of quantum dot-based single photon sources along with near-unity efficient photon collection[149]. D.Riedel, et al. exploited this approach to realize Purcell-enhanced single photon emission from an NV center in a thin single crystal diamond membrane (Fig. 8)[144]. The Fabry-Pérot cavity consists of a plane bottom mirror and a concave top mirror, both of which are distributed Bragg reflectors with reflectivity >99.99%. The curved top mirror is fabricated by creating a concave depression in a silica substrate with laser ablation of a high-power CO_2 laser followed by mirror coating[143]. The 200 nm-thick diamond membrane was prepared by using smart-cut approach. These membranes are subsequently transferred to a planar mirror that is placed on three-axis nanopositioners by using a micromanipulator. They reported Purcell factor for the ZPL of ~30 together with the high Q-factor of 58,500. In addition, S. Häußler et al. demonstrated Purcell enhancement of SiV^- centers in a thin single crystal diamond membrane by using the same manner[145]. They observe cavity-coupled fluorescence from an ensemble of SiV^- centers with an enhancement factor of ~1.9.

Summary of photonic structures

Table 1 summarizes diamond photonic structures with their purposes and features.

Hybrid integration for quantum information science

As reviewed in the previous section, the scalability of integrated diamond photonics is limited by the lack of the technology of fabricating wafer-scale diamond photonic integrated circuits. Thus, the next stage to realize scalable diamond quantum photonics is the hybrid integration of color centers in diamond nanostructures onto a photonic chip based on other materials particularly well-developed photonic materials, including Si, SiN, $LiNbO_3$ and AlN. In this section, we review the hybrid integration of diamond color centers on such photonic chips.

Pick-and-Place

A potential solution for hybrid integration of diamond nanostructures on chips is the use of pick-and-place techniques[34], which offer a viable route to combine color centers with state-of-the-art integrated photonics. Thus far, the hybrid integration of a diamond micro-waveguide containing a single color center onto a SiN and LN waveguide has been demonstrated using a micromanipulator[150,151]. This approach has also been employed for the hybrid integration of various types of quantum emitters (e.g., III–V semiconductor quantum dots, 2D materials, and carbon nanotubes)[36].

The integration of multiple quantum emitters on a single photonic chip is critical for large-scale quantum information processing. Meanwhile, integrating multiple quantum emitters presents several challenges, including inhomogeneities of each emitter, poor device yield, and complex device requirements. Wan et al., solved these issues by the hybrid integration of

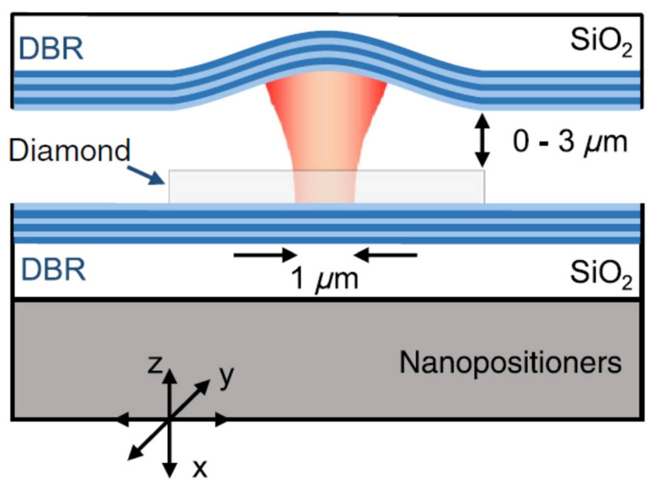

Fig. 8 | Diamond quantum photonics based on a Fabry-Pérot microcavity. The Fabry-Pérot cavity consists of a plane bottom mirror and a concave top mirror, both of which are distributed Bragg reflectors with reflectivity >99.99%. The curved top mirror is fabricated by creating a concave depression in a silica substrate with laser ablation of a high-power CO_2 laser followed by mirror coating. The 200 nm-thick diamond membranes are prepared by using smart-cut approach and subsequently transferred to a planar mirror that is placed on three-axis nanopositioners by using a micromanipulator. DBR: distributed Bragg reflector. Reproduced from ref. 144 under the terms of the Creative Commons Attribution License (CC BY 4.0).

Table 1 | Summary of photonic structures with their purposes and features

Photonic Structure	Purpose	Feature
Waveguide	Guiding light in a photonic chip	Propagation loss: 0.34 dB/cm[196]
Photonic crystal	Light-matter interaction for quantum emitters	Q-factor: 1.8×10^5 (1D), 1.6×10^5 (2D)[136] Mode volume: $0.5 \times \left(\frac{\lambda}{n}\right)^3$ (1D), $2.18 \times \left(\frac{\lambda}{n}\right)^3$ (2D)[136]
Ring resonator	Light-matter interaction for quantum emitters and nonlinear photonics	Q-factor: 1.5×10^5 at telecom[104] Mode volume: $2.3 \times \left(\frac{\lambda}{n}\right)^3$[104]
Microdisk resonator	Light-matter interaction	Q-factor: $>10^5$ at telecom[119] Mode volume: $12.6 \times \left(\frac{\lambda}{n}\right)^3$[119]

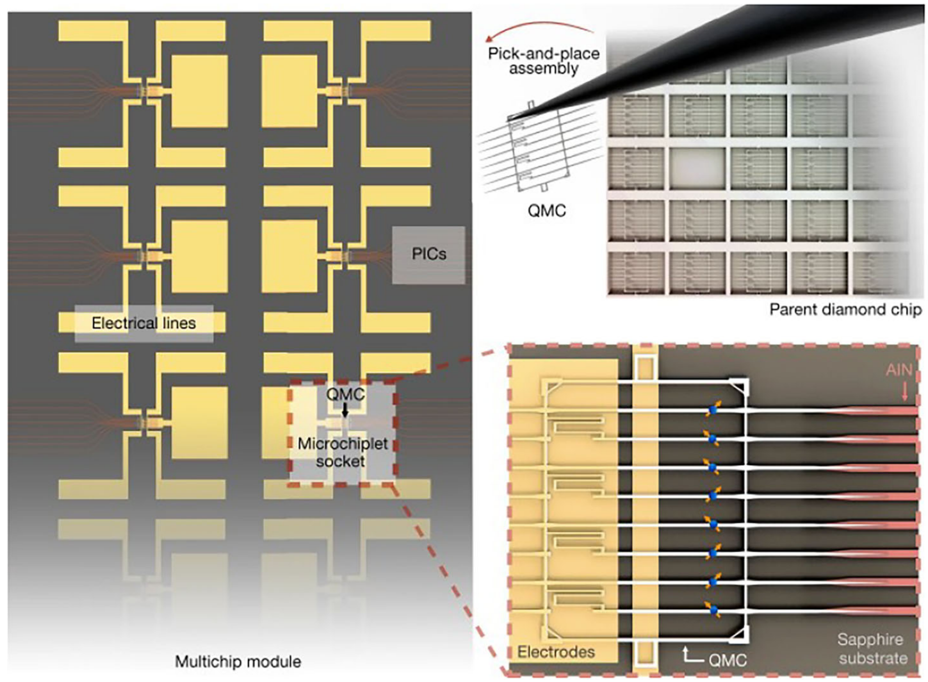

Fig. 9 | Large-scale quantum system assembled by pick-and-place integration of diamond micro-structures. Quantum microchiplets (QMCs) are placed on a photonic integrated circuit (PIC) which is composed of AlN waveguides as optical interfaces and electrodes to control the optical transitions. The chip and QMCs were separately fabricated, followed by an assembly process based on pick-and-place inside SEM system. Reproduced with permission from Springer Nature. Copyright 2020[152].

'quantum microchiplets (QMCs)'—arrays of nanobeams which contain highly coherent quantum emitters—on a photonic chip[152] (Fig. 9). A 128-channel, defect-free diamond array of GeV and SiV centers was successfully integrated on the same AlN-based photonic chip. The integration inside SEM system provided the positional accuracy of their process to be 38 ± 16 nm. Spectral inhomogeneities of each color center in the device were also compensated in situ by strain wavelength tuning.

Nanodiamonds are also promising hosts for quantum emitters and quantum sensors that provide significant versatility in types of integration due to their small size and ease of production[153–155]. In particular, their small size is advantageous for achieving an efficient emitter-cavity interface[156,157]. To scalably fuse nanodiamonds with integrated photonics, several groups have tackled the hybrid integration of nanodiamonds on chip[158–160]. Among them, K. G. Fehler et al. demonstrated the hybrid integration of SiV^- center in nanodiamond onto SiN photonic crystal cavities[161,162]. They employed atomic force microscope nanomanipulation to attain control of spatial and dipole alignment. They achieved a Purcell enhancement of more than 4 on individual optical transitions of SiV^- under on-chip optical excitation. In addition, P. P. J. Schrinner et al. demonstrated the integration of NV centers in diamond on low autofluorescent Ta_2O_5-on-insulator waveguides[163]. They succeeded in achieving both anti-bunching and optically detected magnetic resonance (ODMR). Moreover, H. C. Weng, et al. demonstrated heterogeneous integration of NV centers in nanodiamond with SiN photonics from a standard 180 nm CMOS foundry process[164]. Nanodiamonds in solution are deposited onto the chip, where predefined sites form a regular array on the waveguide. The solvent is then allowed to evaporate, leaving the nanodiamonds in place. Further research into controlling the position, dipole orientation, and quantity of point defects in diamond is essential for scalable quantum photonic applications.

Hybrid GaP-on-diamond approach

We have introduced several recent nanofabrication technologies of diamond in "Breakthrough in diamond nanotechnology". An alternative approach uses a thin waveguiding layer based on GaP ($n = 3.3$) that is formed on diamond surface ($n = 2.4$)[165,166]. This approach allows for chip-scale integration of devices with uniform chip thickness and high yield, which is not easy to achieve by undercutting or thinning the diamond. M. Gould et al. demonstrated the chip-scale transmission measurements for three key components of a GaP-on-diamond integrated photonics platform: waveguide-coupled disk resonators, directional couplers, and grating couplers (Fig. 10)[167]. They also presented proof-of-principle measurements demonstrating NV center emission coupled into selected devices. The potential total quantum efficiency of ZPL photon collection into the bus waveguide in this approach is approximately 33%. Furthermore, GaP exhibits a $\chi^{(2)}$ optical nonlinearity and thus allows for integrated electro-optic switches based on the linear electro-optic effect[168]. The main disadvantage of GaP-on-diamond systems is a reduced interaction between NV centers and guided optical modes due to the relatively small overlap between a GaP photonic mode and NV center. The comparison between hybrid diamond integrated devices and other platforms is summarized in Table 2. We included semiconductor quantum dots (QDs)[169–179] and defects in 2D materials such as WSe_2[180] and hexagonal boron nitride (hBN)[181] in this comparison.

Cryo-CMOS technology

In current solid-state qubit implementations, the challenge is how to coexist the quantum chip in a dilution refrigerator and the room-temperature electronics especially fabricated by CMOS procedure. By elaborating the device design and addressing the heating and power issues, plenty of functionalities have been shown to operate at cryogenic temperature, including optical modulators[182], programmable photonic circuits[183], control of gate-defined quantum dots[184–186], and large-scale superconducting quantum computing[187–189].

Color centers in diamond as quantum emitters and memories are also required to operate at cryogenic temperature. In addition, for most quantum applications, millions of physical qubits are required to encode thousands of logical qubits. To build a fully connected graph state to maximize our use of qubit resources, L. Li et al. introduced a modular quantum system-on-chip architecture that hosts thousands of individually addressable SnV spin qubits in two-dimensional arrays of QMCs (8×8) into a CMOS-based application-specific integrated circuit designed for cryogenic control[190]. The system's codesign with CMOS electronics is advantageous for the compact two-dimensional array of qubit arrangements, qubit inhomogeneous compensation, and system's control elements.

For large-scale heterogeneous integration, they developed lock-and-release heterogeneous integration technology as illustrated in Fig. 11a. This procedure enables the parallel transfer of an 8×8 matrix of quantum

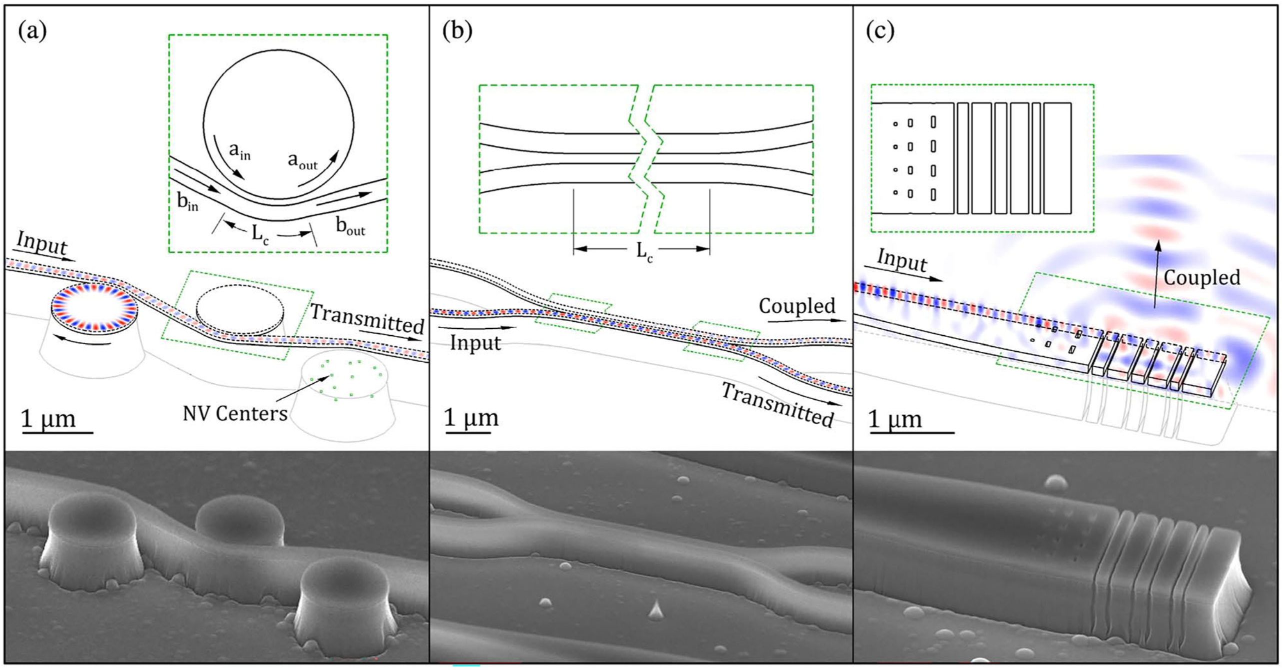

Fig. 10 | Hybrid GaP-on-diamond photonics. Top: schematic views with overlaid finite-difference time-domain (FDTD) simulations. Bottom: SEM images of integrated GaP-on-diamond devices. **a** Waveguide-coupled disk resonators, **b** directional coupler, **c** grating out-coupler. Reproduced with permission from ref. 167. Copyright 2016 Optical Society of America.

Table 2 | Comparison between hybrid diamond devices and other platforms

Refs.	Emitter	Structure	Hybrid integration	Cavity	CMOS-compatible demonstration	$g^{(2)}(0)$	Output	Emitter-chip coupling
150	NV	Diamond μ-WG on SiN WG	MM	N	N	0.07	Edge	43%
167	NV	GaP-on-diamond WG	EG of GaP	Y	N	—	Grating	33%
150	SiV	Diamond NB on LN WG	MM	N	N	0.63	Grating	Diamond–LN transmission: 92%
152	SiV and GeV	Diamond NB arrays on AlN WG	MM	N	N	0.05 (SiV) 0.06 (GeV)	Edge	55%
164	NV	Nanodiamond on SiN WG	MM	N	Y	0.48	Grating	9%
161	SiV	Nanodiamond on SiN PhC-connected WG	MM	Y	N	—	Grating	~4%
169	QD	GaAs NW in SiN WG	MM	N	N	0.07	Edge	12%
170	QD	GaAs NW in SiN WG	MM	N	N	0.13	Edge	12%
171	QD	InP NB on Si WG	MM	N	N	0.25	Grating	Collection: ~3%
172	QD	GaAs NB on SiN WG	MM	N	N	0.07	Edge	31%
173	QD	GaAs PhC on GaAs WG	TP	Y	N	0.23	Grating	63%
174	QD	GaAs PhC on Si WG	TP	Y	Y	0.30	Grating	~70%
175	QD	GaAs PhC on SiN WG	TP	Y	Y	0.1	Grating	53%
176	QD	InP PhC on Si WG	TP	Y	Y	0.20	Grating	~82%
177	QD	GaAs NB on SiN WG	WB	Y	N	0.13	Edge	72%
178	QD	GaAs NB on SiN WG	WB	N	N	0.11	Edge	3%
179	QD	GaAs diode arrays with Si WGs	WB	N	N	0.23	Edge	8%
180	defect	WSe_2 on SiN WG	TP	N	N	0.47	Edge	NA
181	defect	hBN in SiN WG	TP	N	Y	0.22	Edge	12%

EG Epitaxial growth, *LN* Lithium niobate, *MM* Micromanipulation, *NB* Nanobeam, *NW* Nanowire, *TP* Transfer printing, *WB* Wafer bonding, *WG* Waveguide.

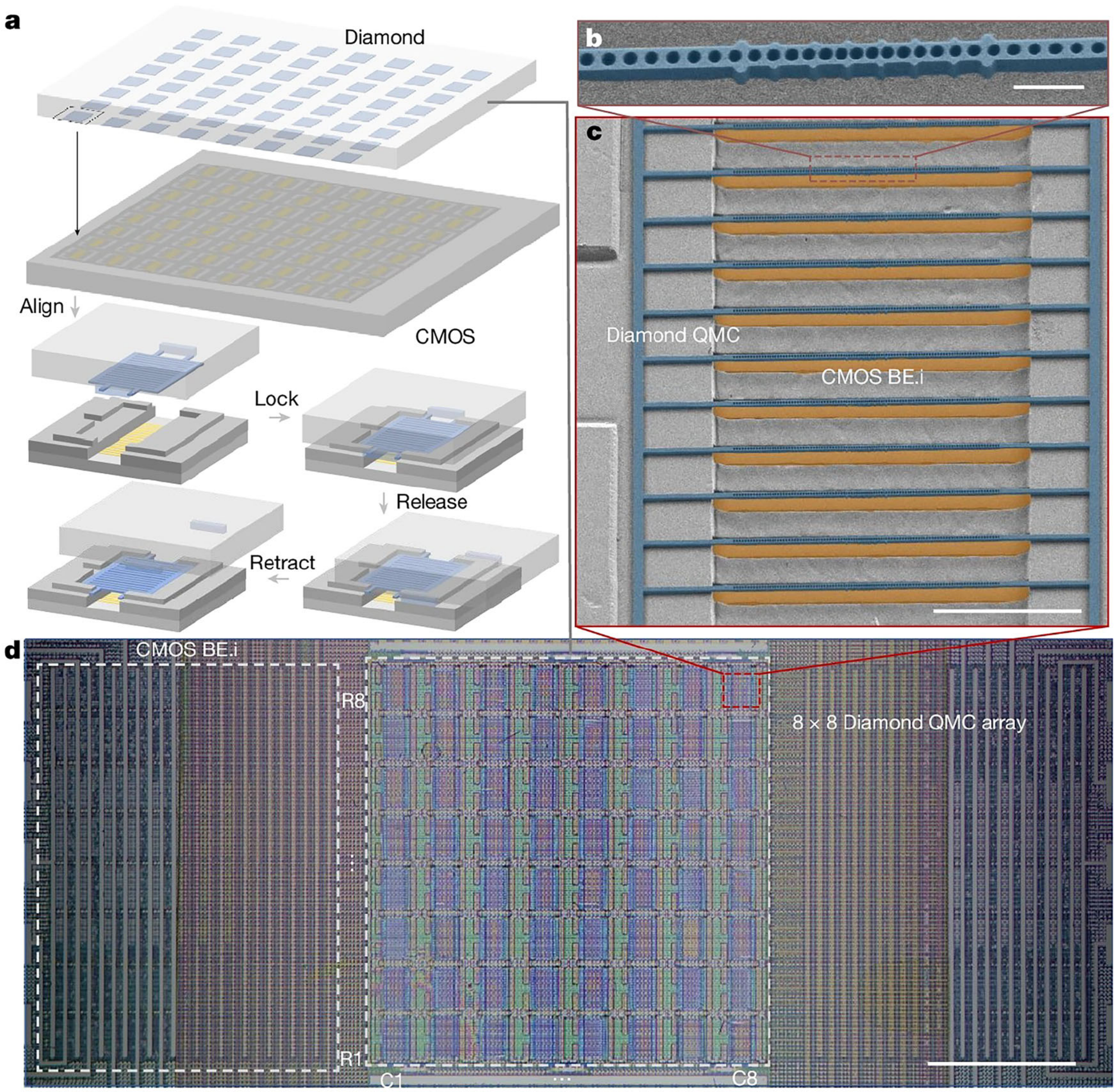

Fig. 11 | Cryo-compatible CMOS application-specific integrated circuit (ASIC) with the parallel-integrated diamond microchiplets. **a** Parallel integration of an 8 × 8 array of diamond QMCs, during which each the QMC is aligned to a CMOS socket, mechanically locked to the socket, broken apart from the mother diamond substrate, and installed with the unity yield at the end. **b** SEM image of a free-space-coupled cavity antenna (scale bar, 1 μm), supported by **c** a diamond QMC on the CMOS socket (scale bar, 10 μm). **d** Optical microscope image of the whole QMC array on the CMOS ASIC. Reproduced with permission from Springer Nature. Copyright 2024[190].

memories to the central region (500 × 500 μm) of the CMOS chip socket that includes 1024 quantum channels in total. First, the diamond parent chip that was placed on a PDMS film attached to a glass slide was flipped and aligned with a locking structure. Subsequently, the QMCs were finely adjusted with two probes, which resulted in the QMC transfer yield of 100%. After alignment, the parent bulk diamond was vertically moved to lock the QMC. Finally, the diamond was horizontally moved and retracted to break the tethers between the QMC and the bulk diamond for release. Figure 11b, c display SEM images of a single central quantum channel and a single QMC region of the chip, respectively. The orange region indicates the individual CMOS backplane electrode region beneath the QMCs. A perturbative cavity design was implemented in each quantum channel as a dielectric antenna optimized for free-space collection, allowing for both a quality factor of 2000 and a collection efficiency of 96% with an NA of 0.9 in simulation. Figure 11d shows an optical microscope image of the 1024 quantum channels integrated into the CMOS control chip. For each quantum channel, we expect to have around three resonant quantum emitters on average at a certain optical frequency. They estimated the average tuning range of around 2 GHz within the applicable voltage range. The number of quantum channels in this design can be readily scaled by means of increased qubit density, larger active regions and optical networking across quantum system-on-chip modules.

Hybrid integration for quantum sensing

In this section, we review the hybrid integration of diamond color centers on chips for practical quantum sensing.

Pick-and-Place method

Among the pick-and-place techniques, transfer printing is promising as a back-end process for the hybrid integration of photonic and electronic components with desirable materials[173,174,191–194]. However, the challenge is the incompatibility of current nanofabrication technology for diamond photonics with existing hybrid integration approaches. For instance, angled etching produces a diamond nanostructure with triangular cross section that is structurally difficult to place on other substrates by using conventional pick-and-place techniques. The bottom of the diamond nanostructure formed through quasi-isotropic etching is even non-flat depending on its width and shape[195]. Thus, the development of hybrid integration techniques with near-unity yields, regardless of the sample structure, is essential for scalable diamond quantum photonics.

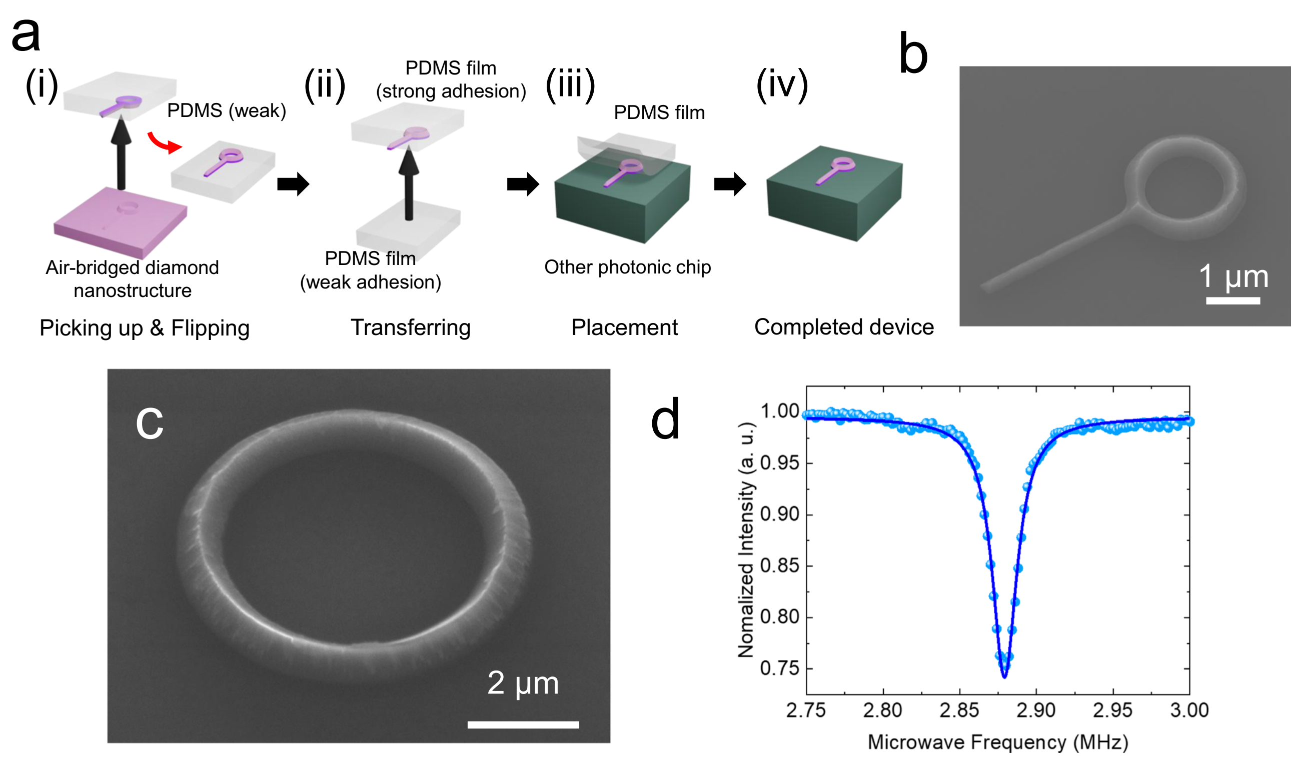

Fig. 12 | Transfer printing based on pick-flip-and-place technique. a Operation flow: (i) picking up air-bridged structure using a PDMS film, (ii) re-picking up the structure from the flipped film, (iii) placing the structure onto an arbitrary substrate, and (iv) completed picture. **b** SEM image of the integrated nanobeam diamond structure, where flat interface is ensured between the structure and the substrate. Reproduced from ref. 106 under the terms of the Creative Commons Attribution License (CC BY 4.0). **c** SEM image of the integrated diamond micro-ring resonator using the same method. **d** Optically detected magnetic resonance spectrum obtained from the ring resonator, reaching the theoretical limit of spin contrast (~25%). Reproduced with permission from ref. 196 under the terms of the Creative Commons Attribution License (CC BY 4.0).

The authors and their peers proposed and demonstrated the deterministic hybrid integration of a diamond NV triangular nanobeam on chip[106]. The proposed "pick-flip-and-place" transfer printing picks up and flips a suitable diamond nanostructure by using a film with weaker adhesion, transfers it to the other film with stronger adhesion, and places it on a photonics chip (Fig. 12a). The advantage of this approach is to provide a flat surface interface between a diamond nanostructure and a photonic chip, enabling us to integrate diamond nanostructures with arbitrary design on chip with near-unity success. Figure 12b shows an SEM image of the integrated nanobeam diamond structure. Notably, the proposed technique can be also applied to hybrid integration of quantum emitters described in the previous section.

The same authors also addressed nanoscale quantum sensing with high field sensitivity by using on-chip diamond micro-ring resonators[196]. They fabricated the ring resonator containing high-density NV centers by using pick-flip-and-place transfer printing, which enables the efficient use of photons by confining them in a nanoscale region (Fig. 12c). The ring resonator possesses a Q-factor of 2000 even containing high-density NV centers. The device yielded the magnetic sensitivity of 1.0 $\mu T/\sqrt{Hz}$ on a photonic chip with a measurement contrast of theoretical limit (~25%) as shown in the optically detected magnetic resonance spectrum of Fig. 12d. They also showed that the proposed on-chip approach can improve sensitivity via efficient light extraction with photonic waveguide coupling.

CMOS-compatible sensing

For practical applications of quantum sensing, it is desirable to make the whole sensor device compact. However, existing systems of diamond quantum sensing involve bulky and discrete off-the-shelf instruments that limit practical applications and scalability of the approach. For example, quantum sensing based on NV centers requires a number of functional components such as excitation laser source, an optical filter to cut off the laser, a microwave generator to manipulate NV spins, and a photodetector. D. Kim et al., demonstrated the integration of NV-based quantum sensors with CMOS electronics to realize a compact and scalable sensor device[197] (Fig. 13a, b). Using standard CMOS technology, they integrated the necessary components for quantum sensing (e.g., microwave antenna, optical filter based on metamaterials, photodetector and so on) in a 200 μm × 200 μm footprint. A 45° cut in the corner of the diamond guides green pump laser from outside to NV centers inside the diamond. This side excitation can suppress the intrusion of laser background into the photodetector located below the diamond. The green laser pump beam is further filtered out by optical filters based on a periodic metal–dielectric structure. An on-chip microwave generator and inductor allow us to manipulate the NV electron spin transitions. The demonstrated field sensitivity of magnetometry was 32 $\mu T/\sqrt{Hz}$.

Compact device for practical applications

To construct compact devices, several groups combined optical fiber with diamond quantum sensing[198–202]. A. Kuwahata et al. demonstrated a compact probe system integrated into a fiber-optics platform to detect the magnetic field generated by magnetic nanoparticles for diagnosis of breast cancer (Fig. 13c)[200]. For efficient lock-in detection of signals from the magnetic nanoparticles, AC magnetic field was generated by the excitation coil of several hundred microteslas, which results in magnetization of magnetic nanoparticles. The minimum detectable AC magnetic field was approximately 57.6 nT for one second measurement time. The device enabled us to detect the micromolar concentration of magnetic nanoparticles at distances of a few millimeters. A compact and portable nanodiamond-based measuring instrument was also recently demonstrated with the field sensitivity of 1.34 $\mu T/\sqrt{Hz}$, operating on the USB 3.0 power supply of a laptop computer[203]. Its portability is achieved through low power consumption in both the optical fiber and microwave components. The

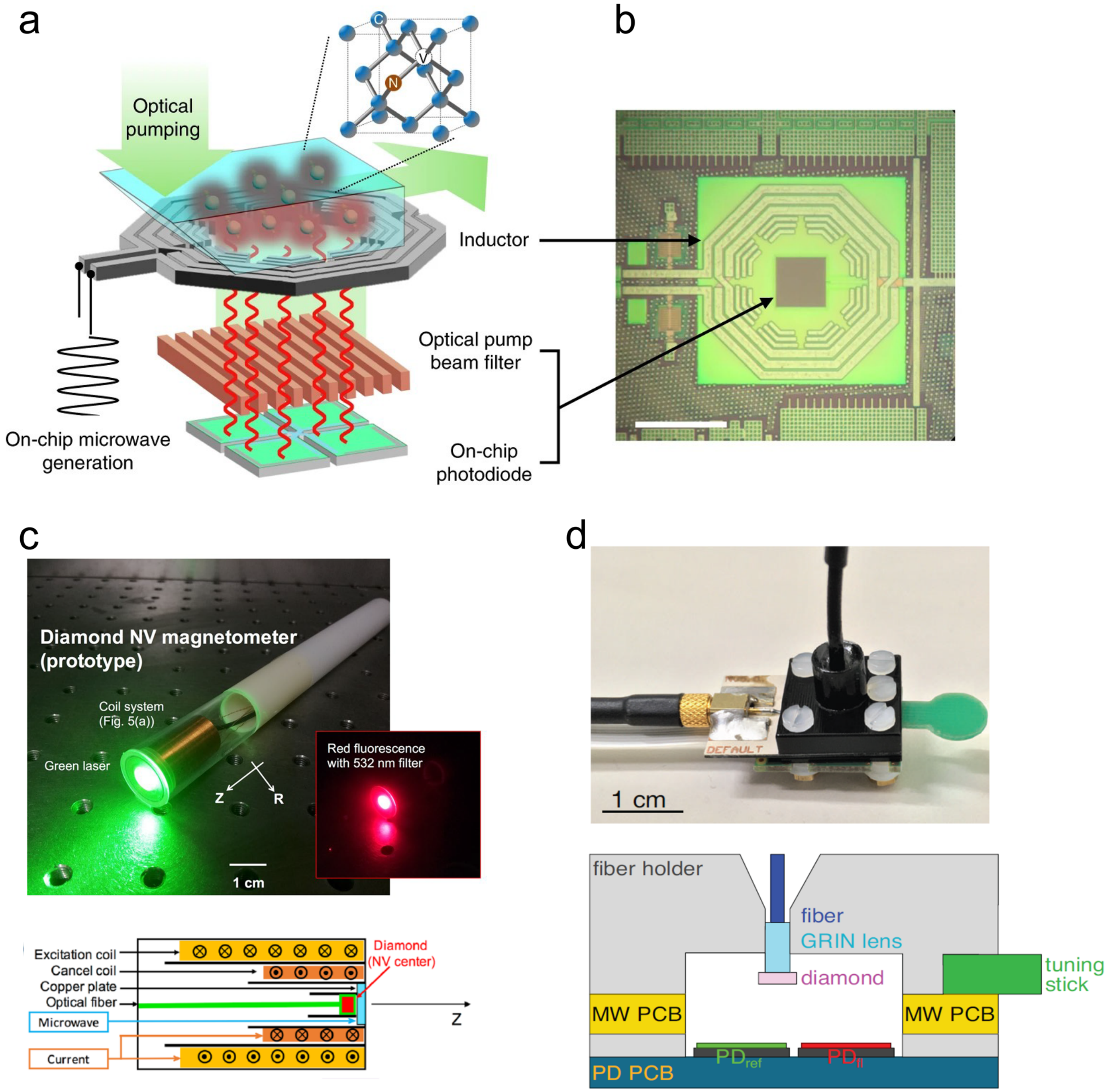

Fig. 13 | Prototypes of a quantum sensing module with small footprints. **a** Configuration of the CMOS-integrated quantum sensor chip. **b** Top view of the chip before the diamond slab is integrated. Reproduced with permission from Springer Nature. Copyright 2019[197]. **c** Fiber-integrated probe system for biomedical applications. An exterior image (top) and the system configuration (bottom). Reproduced from ref. 200 under the terms of the Creative Commons Attribution License (CC BY 4.0). **d** Portable device integrated with a fiber optical input. The device picture (top) and the configuration (bottom). Reproduced from ref. 201 under the terms of the Creative Commons Attribution-NonCommercial-NoDerivatives License (CC BY-NC-ND 4.0)

optics employ a diamond corner cube that enhances the photodiode current by a factor of 2.1 compared to a planar diamond, while the microwave source consumes 20 dB less power thanks to a microwave resonator with a λ/4 open stub that strongly drives the NV center magnetically.

M. Stürner et al. demonstrated a fiber-integrated compact diamond magnetometer (Fig. 13d)[201]. The proposed portable device comprises all necessary components for quantum sensing including offset magnetic field, laser source, microwave generator, and signal processing unit. A single-mode fiber guides the green laser to optically initialize NV centers. deploys a balanced detection scheme built up by two photodetectors augmented close to the diamond. Microwave was sufficiently provided by a split-ring resonator formed by two inductively coupled transmission lines, which were terminated by two capacitive gaps. The bandwidth of the resonator is 23.48 ± 0.08 MHz, and the resonance frequency can be tuned in the range from 2.8 to 3.0 GHz by putting a metallized plate (resonator tuning stick) on the resonator structure. Surprisingly, this portable setup yields a sensitivity of $\approx 344\ \mathrm{pT}/\sqrt{\mathrm{Hz}}$. The comparison between hybrid diamond sensing devices and other quantum devices is summarized in Table 3.

Discussion

The nanofabrication techniques of diamond reviewed above has accelerated the research of quantum technologies based on color centers in diamond. The hybrid integration techniques discussed in this review have also enabled the fusion of high-performance diamond quantum devices with cutting-edge photonic chips. Despite these progresses, there still remain fundamental challenges to construct more complex and larger-scale diamond

Table 3 | Comparison between hybrid diamond sensing devices and other quantum devices

Refs.	Platform	Operation temperature	Sensitivity	Device size
197	NV center	Room temperature	$32\ \mu T/\sqrt{Hz}$	200 μm × 200 μm
198	NV center	Room temperature	$7\ nT/\sqrt{Hz}$	$1.1 \times 0.7 \times 0.7\ m^3$
199	NV center	Room temperature	$310\ pT/\sqrt{Hz}$	$0.44 \times 0.55 \times 0.6\ m^3$
200	NV center	Room temperature	57.6 nT	Several centimeters
201	NV center	Room temperature	$344\ pT/\sqrt{Hz}$	$35 \times 110 \times 120\ mm^3$
202	NV center	Room temperature	$44\ pT/\sqrt{Hz}$	$63 \times 47 \times 21\ mm^3$
255	SQUID	Cryogenic temperature	A few $fT/\sqrt{Hz}$	Several meters
256	OPM	Room temperature	$10\ fT/\sqrt{Hz}$	$2 \times 2 \times 5\ cm^3$

quantum photonic devices. In this section, we will discuss the short-term and long-term challenges for quantum applications based on diamonds.

Challenges in quantum information processing

A short-term goal for this field is how to precisely control quantum emitters. We reviewed several ways to create color centers in diamonds in "Creation of color centers in diamond". However, each approach has different challenges including position accuracy, yields, and dipole orientation. Especially, NV centers are required to be positioned at the exact center of photonic cavities to obtain efficient ZPL collection. We believe that the combination of smart-cut technique with delta-doped layer would solve this issue and enable the creation of high-quality photonic cavities hosting perfectly position-controlled NV centers. Another issue is broadening of the linewidth of NV centers caused by charge-state instability when they are positioned near the diamond surface[204]. This issue can be mitigated through chemical treatments such as surface passivation[205], termination[206], doping[207], and the introduction of graphene[208]. Alternatively, the use of group IV-based color centers is promising, as they are insensitive to electric field fluctuations due to the absence of a permanent electric dipole, which arises from the inversion-symmetric D_{3d} structure of the defect. The frequency stabilization of SiV centers has also been reported through electromechanical strain control[209].

A long-term goal of diamond-based quantum information processing is scalability, such as (i) the wafer-scale process of diamond nanofabrication and (ii) massive hybrid integration. The smart-cut approach with wafer-scale growth of diamond would be the most promising way to massively fabricate high-quality diamond nanostructures. Massive integration would be also possible by developing transfer printing technique with automated operation[210] and in parallel manner[211]. The other challenge of scalable diamond quantum photonics is to implement additional functions on chip for future quantum applications, such as electrical excitation[10,212], excitation through a waveguide[213–215], and efficient chip-to-fiber interface[176,216–218]. Controlling the properties of NV centers is also crucial, including the manipulation of the charge state between neutral and negatively charged NV centers[219–227] and spectral tuning[228–232].

Challenges in quantum sensing

As introduced in "Creation of color centers in diamond", quantum sensing has a wide range of applications, spanning from fundamental physics to medical fields. For a near-term goal in quantum sensing, improving factors such as extraction efficiency of NV emissions, spin coherence time, and photoluminescence contrast is crucial for any applications with higher sensitivity. Improvement of coherence time is addressed in various ways including decoupling techniques[233–236], surface treatments[237,238], and material synthesis[239]. Photoluminescence contrast could also be enhanced by perfectly aligning NV orientations[240,241] or inducing stimulated emission[242–245]. We note that quantum defects in hBN have recently emerged as alternative solid-state quantum sensors in atomic scale[246,247]. Investigation and development of such novel materials are also imperative for broadening the applications of quantum sensing.

One of the ultimate goals in quantum sensing is to construct compact sensor devices with excellent performance. To this end, a number of functional components are required to be integrated on a single photonic chip. Design of the device needs to be tailored to its intended applications, such as fundamental physics research, NMR and MRI measurements, and medical diagnosis. Diamond photonic nanostructures offer significant advantages for all of these applications, as they have the potential to enable highly sensitive quantum sensing[248]. Recent advancements in metasurfaces will also be incorporated to further miniaturize the device[249–251]. Furthermore, future scalable and high-throughput fabrication of diamond quantum sensors might allow for monitoring electric vehicle batteries[252], sensing in microfluidics systems[253], and detecting dark matters[254]. These increasing demands will accelerate the development of truly practical diamond quantum sensors.

Conclusion

A review of recent progress regarding the development of hybrid diamond quantum photonics platforms was presented. A brief explanation of the techniques for creating color centers in diamond, as well as the fabrication methods for diamond nanostructures, is provided. We reviewed the hybrid integration of diamond color centers on chips for quantum information processing and practical quantum sensing. The review concludes with a discussion of the challenges and perspectives in diamond quantum photonics. We emphasize that the advantage of hybrid integration lies in the ability to integrate diamond quantum components after their optimization and sophistication. Although numerous challenges persist, the hybrid integration approach, combined with recent advancements in diamond nanofabrication techniques, is poised to elevate diamond quantum technologies to the next level.

Received: 7 November 2024; Accepted: 17 March 2025;
Published online: 08 May 2025

References

1. Aharonovich, I., Greentree, A. D. & Prawer, S. Diamond photonics. *Nat. Photon* **5**, 397–405 (2011).
2. Aharonovich, I., Englund, D. & Toth, M. Solid-state single-photon emitters. *Nat. Photon* **10**, 631–641 (2016).
3. Barry, J. F. et al. Sensitivity optimization for NV-diamond magnetometry. *Rev. Mod. Phys.* **92**, 015004 (2020).
4. Rembold, P. et al. Introduction to quantum optimal control for quantum sensing with nitrogen-vacancy centers in diamond. *Avs Quantum Sci.* **2**, 024701 (2020).
5. Lee, J. et al. Integrated single photon emitters. *AVS Quantum Sci.* **2**, 031701 (2020).
6. Awschalom, D. et al. Development of Quantum Interconnects (QuICs) for next-generation information technologies. *PRX Quantum* **2**, 017002 (2021).
7. Ruf, M., Wan, N. H., Choi, H., Englund, D. & Hanson, R. Quantum networks based on color centers in diamond. *J. Appl. Phys.* **130**, 070901 (2021).

8. Hu, X.-M., Guo, Y., Liu, B.-H., Li, C.-F. & Guo, G.-C. Progress in quantum teleportation. *Nat. Rev. Phys.* **5**, 339–353 (2023).
9. Wolfowicz, G. et al. Quantum guidelines for solid-state spin defects. *Nat. Rev. Mater.* **6**, 906–925 (2021).
10. Mizuochi, N. et al. Electrically driven single-photon source at room temperature in diamond. *Nat. Photon* **6**, 299–303 (2012).
11. Pompili, M. et al. Realization of a multinode quantum network of remote solid-state qubits. *Science* **372**, 259–264 (2021).
12. Gschwendtner, M., Bormuth, Y., Soller, H., Stein, A. & Walsworth, R. L. Quantum sensing can already make a difference. But Where? *J. Innov. Manag.* **12**, I–XI (2024).
13. Maze, J. R. et al. Nanoscale magnetic sensing with an individual electronic spin in diamond. *Nature* **455**, 644–647 (2008).
14. Steinert, S. et al. High sensitivity magnetic imaging using an array of spins in diamond. *Rev. Sci. Instrum.* **81**, 043705 (2010).
15. Wolf, T. et al. Subpicotesla diamond magnetometry. *Phys. Rev. X* **5**, 041001 (2015).
16. Dolde, F. et al. Electric-field sensing using single diamond spins. *Nat. Phys.* **7**, 459–463 (2011).
17. Kucsko, G. et al. Nanometre-scale thermometry in a living cell. *Nature* **500**, 54–58 (2013).
18. Fujiwara, M. et al. Real-time nanodiamond thermometry probing in vivo thermogenic responses. *Sci. Adv.* **6**, aba9636 (2020).
19. Segawa, T. F. & Igarashi, R. Nanoscale quantum sensing with Nitrogen-Vacancy centers in nanodiamonds - A magnetic resonance perspective. *Prog. Nucl. Magn. Reson. Spectrosc.* **134-135**, 20–38 (2023).
20. Aslam, N. et al. Quantum sensors for biomedical applications. *Nat. Rev. Phys.* **5**, 157–169 (2023).
21. Du, J., Shi, F., Kong, X., Jelezko, F. & Wrachtrup, J. Single-molecule scale magnetic resonance spectroscopy using quantum diamond sensors. *Rev. Mod. Phys.* **96**, 025001 (2024).
22. Casola, F., van der Sar, T. & Yacoby, A. Probing condensed matter physics with magnetometry based on nitrogen-vacancy centres in diamond. *Nat. Rev. Mater.* **3**, 17088 (2018).
23. Lee-Wong, E. et al. Nanoscale detection of magnon excitations with variable wavevectors through a quantum spin sensor. *Nano Lett.* **20**, 3284–3290 (2020).
24. Li, Y. et al. A fiber-coupled scanning magnetometer with nitrogen-vacancy spins in a diamond nanobeam. *ACS Photonics* **10**, 1859–1865 (2023).
25. Schröder, T. et al. Quantum nanophotonics in diamond [Invited]. *J. Opt. Soc. Am. B* **33**, B65 (2016).
26. Janitz, E., Bhaskar, M. K. & Childress, L. Cavity quantum electrodynamics with color centers in diamond. *Optica* **7**, 1232–1252 (2020).
27. Shandilya, P. K. et al. Diamond integrated quantum nanophotonics: spins, photons and phonons. *J. Lightwave Technol.* **40**, 7538–7571 (2022).
28. Moody, G. et al. 2022 Roadmap on integrated quantum photonics. *J. Phys. Photonics* **4**, 012501 (2022).
29. Becher, C. et al. 2023 roadmap for materials for quantum technologies. *Mater. Quantum Technol.* **3**, 012501 (2023).
30. Cacciapuoti, A. S. et al. Quantum internet: networking challenges in distributed quantum computing. *IEEE Netw.* **34**, 137–143 (2020).
31. Wehner, S., Elkouss, D. & Hanson, R. Quantum internet: a vision for the road ahead. *Science* **362**, eaam9288 (2018).
32. Beukers, H. K. C. et al. Remote-Entanglement protocols for stationary qubits with photonic interfaces. *PRX Quantum* **5**, 010202 (2024).
33. Chia, C. et al. Diamond quantum nanophotonics and optomechanics. in *Diamond for Quantum Applications Part 2* (Academic Press, 2021).
34. Elshaari, A. W., Pernice, W., Srinivasan, K., Benson, O. & Zwiller, V. Hybrid integrated quantum photonic circuits. *Nat. Photon* **14**, 285 (2020).
35. Kim, J.-H., Aghaeimeibodi, S., Carolan, J., Englund, D. & Waks, E. Hybrid integration methods for on-chip quantum photonics. *Optica* **7**, 291–308 (2020).
36. Katsumi, R., Ota, Y. & Benyoucef, M. Telecom-band quantum dots compatible with silicon photonics for photonic quantum applications. *Adv. Quantum Technol.* **2024**, 2300423 (2024).
37. Silverstone, J. W., Bonneau, D., O'Brien, J. L. & Thompson, M. G. Silicon Quantum Photonics. *IEEE J. Sel. Top. Quantum Electron.* **22**, 390–402 (2016).
38. Adcock, J. C. et al. Advances in Silicon Quantum Photonics. *IEEE J. Sel. Top. Quantum Electron.* **27**, 1–24 (2021).
39. Moss, D. J., Morandotti, R., Gaeta, A. L. & Lipson, M. New CMOS-compatible platforms based on silicon nitride and Hydex for nonlinear optics. *Nat. Photon* **7**, 597–607 (2013).
40. Ji, X. et al. Ultra-Low-Loss Silicon Nitride photonics based on deposited films compatible with foundries. *Laser Photonics Rev.* **17**, 2200544 (2023).
41. Liu, J. et al. High-yield, wafer-scale fabrication of ultralow-loss, dispersion-engineered silicon nitride photonic circuits. *Nat. Commun.* **12**, 2236 (2021).
42. Doherty, M. W. et al. The nitrogen-vacancy colour centre in diamond. *Phys. Rep.* **528**, 1–45 (2013).
43. Bradac, C., Gao, W., Forneris, J., Trusheim, M. E. & Aharonovich, I. Quantum nanophotonics with group IV defects in diamond. *Nat. Commun.* **10**, 5625 (2019).
44. Iwasaki, T. Color centers based on heavy group-IV elements. in *Diamond for Quantum Applications Part 1* (Academic Press, 2020).
45. Maze, J. R. et al. Properties of nitrogen-vacancy centers in diamond: the group theoretic approach. *N. J. Phys.* **13**, 025025 (2011).
46. Kurtsiefer, C., Mayer, S., Zarda, P. & Weinfurter, H. Stable solid-state source of single photons. *Phys. Rev. Lett.* **85**, 290–293 (2000).
47. Bernien, H. et al. Heralded entanglement between solid-state qubits separated by three metres. *Nature* **497**, 86–90 (2013).
48. Hensen, B. et al. Loophole-free Bell inequality violation using electron spins separated by 1.3 kilometres. *Nature* **526**, 682–686 (2015).
49. Kalb, N. et al. Entanglement distillation between solid-state quantum network nodes. *Science* **356**, 928–932 (2017).
50. Humphreys, P. C. et al. Deterministic delivery of remote entanglement on a quantum network. *Nature* **558**, 268–273 (2018).
51. Hermans, S. L. N. et al. Entangling remote qubits using the single-photon protocol: an in-depth theoretical and experimental study. *N. J. Phys.* **25**, 013011 (2023).
52. Bradley, C. E. et al. A Ten-Qubit solid-state spin register with quantum memory up to one minute. *Phys. Rev. X* **9**, 031045 (2019).
53. Maletinsky, P. et al. A robust scanning diamond sensor for nanoscale imaging with single nitrogen-vacancy centres. *Nat. Nanotechnol.* **7**, 320–324 (2012).
54. Shields, B. J., Unterreithmeier, Q. P., de Leon, N. P., Park, H. & Lukin, M. D. Efficient readout of a single spin state in diamond via spin-to-charge conversion. *Phys. Rev. Lett.* **114**, 136402 (2015).
55. Thiel, L. et al. Probing magnetism in 2D materials at the nanoscale with single-spin microscopy. *Science* **364**, 973–976 (2019).
56. Li, S. et al. Observation of stacking engineered magnetic phase transitions within moire supercells of twisted van der Waals magnets. *Nat. Commun.* **15**, 5712 (2024).
57. Du, C. et al. Control and local measurement of the spin chemical potential in a magnetic insulator. *Science* **357**, 195–198 (2017).
58. Grinolds, M. S. et al. Subnanometre resolution in three-dimensional magnetic resonance imaging of individual dark spins. *Nat. Nanotechnol.* **9**, 279–284 (2014).
59. Lovchinsky, I. et al. Nuclear magnetic resonance detection and spectroscopy of single proteins using quantum logic. *Science* **351**, 836–841 (2016).
60. Hsieh, S. et al. Imaging stress and magnetism at high pressures using a nanoscale quantum sensor. *Science* **366**, 1349–1354 (2019).

61. Bhattacharyya, P. et al. Imaging the Meissner effect in hydride superconductors using quantum sensors. *Nature* **627**, 73–79 (2024).
62. Lesik, M. et al. Magnetic measurements on micrometer-sized samples under high pressure using designed NV centers. *Science* **366**, 1359–1362 (2019).
63. Barry, J. F. et al. Sensitive ac and dc magnetometry with nitrogen-vacancy-center ensembles in diamond. *Phys. Rev. Appl.* **22**, 044069 (2024).
64. Zhao, Z. et al. Sub-nanotesla sensitivity at the nanoscale with a single spin. *Natl Sci. Rev.* **10**, nwad100 (2023).
65. Le Sage, D. et al. Optical magnetic imaging of living cells. *Nature* **496**, 486–489 (2013).
66. Steinert, S. et al. Magnetic spin imaging under ambient conditions with sub-cellular resolution. *Nat. Commun.* **4**, 1607 (2013).
67. Barry, J. F. et al. Optical magnetic detection of single-neuron action potentials using quantum defects in diamond. *Proc. Natl. Acad. Sci. USA* **113**, 14133–14138 (2016).
68. Webb, J. L. et al. Detection of biological signals from a live mammalian muscle using an early stage diamond quantum sensor. *Sci. Rep.* **11**, 2412 (2021).
69. Arai, K. et al. Millimetre-scale magnetocardiography of living rats with thoracotomy. *Commun. Phys.* **5**, 200 (2022).
70. Ledbetter, M. P., Jensen, K., Fischer, R., Jarmola, A. & Budker, D. Gyroscopes based on nitrogen-vacancy centers in diamond. *Phys. Rev. A* **86**, 052116 (2012).
71. Glenn, D. R. et al. Micrometer-scale magnetic imaging of geological samples using a quantum diamond microscope. *Geochem. Geophys. Geosyst.* **18**, 3254–3267 (2017).
72. Stas, P. J. et al. Robust multi-qubit quantum network node with integrated error detection. *Science* **378**, 557–560 (2022).
73. Knaut, C. M. et al. Entanglement of nanophotonic quantum memory nodes in a telecom network. *Nature* **629**, 573–578 (2024).
74. Rosenthal, E. I. et al. Microwave spin control of a tin-vacancy qubit in diamond. *Phys. Rev. X* **13**, 031022 (2023).
75. Iwasaki, T. et al. Tin-vacancy quantum emitters in diamond. *Phys. Rev. Lett.* **119**, 253601 (2017).
76. Wang, P. et al. Transform-limited photon emission from a lead-vacancy center in diamond above 10 K. *Phys. Rev. Lett.* **132**, 073601 (2024).
77. Trusheim, M. E. et al. Lead-related quantum emitters in diamond. *Phys. Rev. B* **99**, 075430 (2019).
78. Ziegler, J. F. Srim-2003. *Nucl. Instrum. Methods Phys. Res. Sect. B: Beam Interact. Mater. At.* **219**, 1027–1036 (2004).
79. Schukraft, M. et al. Invited Article: precision nanoimplantation of nitrogen vacancy centers into diamond photonic crystal cavities and waveguides. *APL Photonics* **1**, 020801 (2016).
80. Lesik, M. et al. Maskless and targeted creation of arrays of colour centres in diamond using focused ion beam technology. *Phys. Status Solidi* **210**, 2055–2059 (2013).
81. Tamura, S. et al. Array of bright silicon-vacancy centers in diamond fabricated by low-energy focused ion beam implantation. *Appl. Phys. Express* **7**, 115201 (2014).
82. Schroder, T. et al. Scalable focused ion beam creation of nearly lifetime-limited single quantum emitters in diamond nanostructures. *Nat. Commun.* **8**, 15376 (2017).
83. Höflich, K. et al. Roadmap for focused ion beam technologies. *Appl. Phys. Rev.* **10**, 041311 (2023).
84. Chen, Y.-C. et al. Laser writing of coherent colour centres in diamond. *Nat. Photon* **11**, 77–80 (2016).
85. Stephen, C. J. et al. Deep three-dimensional solid-state qubit arrays with long-lived spin coherence. *Phys. Rev. Appl.* **12**, 064005 (2019).
86. Chen, Y.-C. et al. Laser writing of individual nitrogen-vacancy defects in diamond with near-unity yield. *Optica* **6**, 662 (2019).
87. Ohno, K. et al. Engineering shallow spins in diamond with nitrogen delta-doping. *Appl Phys. Lett.* **101**, 082413 (2012).
88. Lee, J. C. et al. Deterministic coupling of delta-doped nitrogen vacancy centers to a nanobeam photonic crystal cavity. *Appl Phys. Lett.* **105**, 261101 (2014).
89. Jaffe, T. et al. Novel ultra localized and dense nitrogen delta-doping in diamond for advanced quantum sensing. *Nano Lett.* **20**, 3192–3198 (2020).
90. Bogdanov, S. A. et al. Optical investigation of as-grown NV centers in heavily nitrogen doped delta layers in CVD diamond. *Mater. Today Commun.* **24**, 101019 (2020).
91. Hughes, L. B. et al. Two-dimensional spin systems in PECVD-grown diamond with tunable density and long coherence for enhanced quantum sensing and simulation. *APL Mater.* **11**, 021101 (2023).
92. Schreck, M., Gsell, S., Brescia, R. & Fischer, M. Ion bombardment induced buried lateral growth: the key mechanism for the synthesis of single crystal diamond wafers. *Sci. Rep.* **7**, 44462 (2017).
93. Rondin, L. et al. Magnetometry with nitrogen-vacancy defects in diamond. *Rep. Prog. Phys.* **77**, 056503 (2014).
94. Faraon, A., Barclay, P. E., Santori, C., Fu, K.-M. C. & Beausoleil, R. G. Resonant enhancement of the zero-phonon emission from a colour centre in a diamond cavity. *Nat. Photon.* **5**, 301–305 (2011).
95. Faraon, A. et al. Quantum photonic devices in single-crystal diamond. *N. J. Phys.* **15**, 025010 (2013).
96. Hausmann, B. J. M., Bulu, I., Venkataraman, V., Deotare, P. & Lončar, M. Diamond nonlinear photonics. *Nat. Photon* **8**, 369–374 (2014).
97. Hausmann, B. J. et al. Integrated high-quality factor optical resonators in diamond. *Nano Lett.* **13**, 1898–1902 (2013).
98. Hausmann, B. J. et al. Integrated diamond networks for quantum nanophotonics. *Nano Lett.* **12**, 1578–1582 (2012).
99. Hausmann, B. J. et al. Coupling of NV centers to photonic crystal nanobeams in diamond. *Nano Lett.* **13**, 5791–5796 (2013).
100. Li, L. et al. Coherent spin control of a nanocavity-enhanced qubit in diamond. *Nat. Commun.* **6**, 6173 (2015).
101. Faraon, A., Santori, C., Huang, Z., Acosta, V. M. & Beausoleil, R. G. Coupling of nitrogen-vacancy centers to photonic crystal cavities in monocrystalline diamond. *Phys. Rev. Lett.* **109**, 033604 (2012).
102. Kuruma, K. et al. Telecommunication-wavelength two-dimensional photonic crystal cavities in a thin single-crystal diamond membrane. *Appl Phys. Lett.* **119**, 171106 (2021).
103. Burek, M. J. et al. Free-standing mechanical and photonic nanostructures in single-crystal diamond. *Nano Lett.* **12**, 6084–6089 (2012).
104. Burek, M. J. et al. High quality-factor optical nanocavities in bulk single-crystal diamond. *Nat. Commun.* **5**, 5718 (2014).
105. Jeon, S.-W. et al. Bright Nitrogen-Vacancy Centers in Diamond Inverted Nanocones. *ACS Photon.* **7**, 2739–2747 (2020).
106. Katsumi, R. et al. Hybrid integration of ensemble nitrogen-vacancy centers in single-crystal diamond based on pick-flip-and-place transfer printing. *Appl Phys. Lett.* **123**, 111108 (2023).
107. Maity, S. et al. Spectral alignment of single-photon emitters in diamond using strain gradient. *Phys. Rev. Appl.* **10**, 024050 (2018).
108. Shams-Ansari, A. et al. Supercontinuum generation in angle-etched diamond waveguides. *Opt. Lett.* **44**, 4056–4059 (2019).
109. Cranwell Schaeper, O. et al. Fabrication of photonic resonators in bulk 4H-SiC. *Adv. Mater. Technol.* **6**, 2100589 (2021).
110. Babin, C. et al. Fabrication and nanophotonic waveguide integration of silicon carbide colour centres with preserved spin-optical coherence. *Nat. Mater.* **21**, 67–73 (2022).
111. Sohn, Y.-I., Miller, R., Venkataraman, V. & Lončar, M. Mechanical and optical nanodevices in single-crystal quartz. *Appl. Phys. Lett.* **111**, 263103 (2017).
112. Gough, G. P. et al. Faraday-cage-assisted etching of suspended gallium nitride nanostructures. *AIP Adv.* **10**, 055319 (2020).
113. Latawiec, P., Burek, M. J., Sohn, Y.-I. & Lončar, M. Faraday cage angled-etching of nanostructures in bulk dielectrics. *J. Vac. Sci. Technol. B* **34**, 041801 (2016).

114. Nguyen, C. T. et al. An integrated nanophotonic quantum register based on silicon-vacancy spins in diamond. *Phys. Rev. B* **100**, 165428 (2019).
115. Atikian, H. A. et al. Freestanding nanostructures via reactive ion beam angled etching. *APL Photon.* **2**, 051301 (2017).
116. Atikian, H. A. et al. Diamond mirrors for high-power continuous-wave lasers. *Nat. Commun.* **13**, 2610 (2022).
117. Bhaskar, M. K. et al. Experimental demonstration of memory-enhanced quantum communication. *Nature* **580**, 60–64 (2020).
118. Nguyen, C. T. et al. Quantum network nodes based on diamond qubits with an efficient nanophotonic interface. *Phys. Rev. Lett.* **123**, 183602 (2019).
119. Khanaliloo, B., Mitchell, M., Hryciw, A. C. & Barclay, P. E. High-Q/V monolithic diamond microdisks fabricated with quasi-isotropic etching. *Nano Lett.* **15**, 5131 (2015).
120. Dory, C. et al. Inverse-designed diamond photonics. *Nat. Commun.* **10**, 3309 (2019).
121. Mitchell, M., Lake, D. P. & Barclay, P. E. Realizing Q > 300 000 in diamond microdisks for optomechanics via etch optimization. *APL Photon.* **4**, 016101 (2019).
122. Arjona Martinez, J. et al. Photonic indistinguishability of the Tin-Vacancy center in nanostructured diamond. *Phys. Rev. Lett.* **129**, 173603 (2022).
123. Mouradian, S., Wan, N. H., Schröder, T. & Englund, D. Rectangular photonic crystal nanobeam cavities in bulk diamond. *Appl Phys. Lett.* **111**, 021103 (2017).
124. Kuruma, K. et al. Coupling of a single tin-vacancy center to a photonic crystal cavity in diamond. *Appl Phys. Lett.* **118**, 230601 (2021).
125. Rugar, A. E. et al. Quantum photonic interface for tin-vacancy centers in diamond. *Phys. Rev. X* **11**, 031021 (2021).
126. Pasini, M. et al. Nonlinear quantum photonics with a tin-vacancy center coupled to a one-dimensional diamond waveguide. *Phys. Rev. Lett.* **133**, 023603 (2024).
127. Kuruma, K. et al. Controlling interactions between high-frequency phonons and single quantum systems using phononic crystals. *Nat. Phys.* **21**, 77–82 (2024).
128. Wan, N. H., Mouradian, S. & Englund, D. Two-dimensional photonic crystal slab nanocavities on bulk single-crystal diamond. *Appl. Phys. Lett.* **112**, 141102 (2018).
129. Parikh, N. R. et al. Single-crystal diamond plate liftoff achieved by ion implantation and subsequent annealing. *Appl Phys. Lett.* **61**, 3124–3126 (1992).
130. Fairchild, B. A. et al. Fabrication of ultrathin single-crystal diamond membranes. *Adv. Mater.* **20**, 4793–4798 (2008).
131. Lee, J. C., Magyar, A. P., Bracher, D. O., Aharonovich, I. & Hu, E. L. Fabrication of thin diamond membranes for photonic applications. *Diam. Relat. Mater.* **33**, 45–48 (2013).
132. Gaathon, O. et al. Planar fabrication of arrays of ion-exfoliated single-crystal-diamond membranes with nitrogen-vacancy color centers. *Opt. Mater.* **35**, 361–365 (2013).
133. Magyar, A. P. et al. Fabrication of thin, luminescent, single-crystal diamond membranes. *Appl. Phys. Lett.* **99**, (2011).
134. Guo, X. et al. Tunable and transferable diamond membranes for integrated quantum technologies. *Nano Lett.* **21**, 10392–10399 (2021).
135. Guo, X. et al. Direct-bonded diamond membranes for heterogeneous quantum and electronic technologies. *Nat. Commun.* **15**, 8788 (2024).
136. Ding, S. W. et al. High-Q cavity interface for color centers in thin film diamond. *Nat. Commun.* **15**, 6358 (2024).
137. Fukumoto, S. et al. Heterogeneous direct bonding of diamond and semiconductor substrates using NH_3/H_2O_2 cleaning. *Appl. Phys. Lett.* **117**, 201601 (2020).
138. Liang, J. et al. Fabrication of GaN/Diamond heterointerface and interfacial chemical bonding state for highly efficient device design. *Adv. Mater.* **33**, e2104564 (2021).
139. Yang, C. et al. Large-scale fabrication of surface SiV− centers in a flexible diamond membrane. *Carbon* **203**, 842–846 (2023).
140. Xie, Y. et al. Diamond thin films integrated with flexible substrates and their physical, chemical and biological characteristics. *J. Phys. D Appl. Phys.* **54**, 384004 (2021).
141. Jing, J. et al. Scalable production of ultraflat and ultraflexible diamond membrane. *Nature* **636**, 627–634 (2024).
142. Najer, D. et al. A gated quantum dot strongly coupled to an optical microcavity. *Nature* **575**, 622–627 (2019).
143. Barbour, R. J. et al. A tunable microcavity. *J. Appl. Phys.* **110**, 053107 (2011).
144. Riedel, D. et al. Deterministic enhancement of coherent photon generation from a nitrogen-vacancy center in ultrapure diamond. *Phys. Rev. X* **7**, 031040 (2017).
145. Häußler, S. et al. Diamond photonics platform based on silicon vacancy centers in a single-crystal diamond membrane and a fiber cavity. *Phys. Rev. B* **99**, 165310 (2019).
146. Vogl, T., Lecamwasam, R., Buchler, B. C., Lu, Y. & Lam, P. K. Compact cavity-enhanced single-photon generation with hexagonal boron nitride. *ACS Photon.* **6**, 1955–1962 (2019).
147. Häußler, S. et al. Tunable fiber-cavity enhanced photon emission from defect centers in hBN. *Adv. Opt. Mater.* **9**, 165310 (2021).
148. Wang, D. et al. Turning a molecule into a coherent two-level quantum system. *Nat. Phys.* **15**, 483–489 (2019).
149. Tomm, N. et al. A bright and fast source of coherent single photons. *Nat. Nanotechnol.* **16**, 399–403 (2021).
150. Mouradian, S. L. et al. Scalable integration of long-lived quantum memories into a photonic circuit. *Phys. Rev. X* **5**, 031009 (2015).
151. Riedel, D. et al. Efficient photonic integration of diamond color centers and thin-film lithium niobate. *ACS Photon.* **10**, 4236–4243 (2023).
152. Wan, N. H. et al. Large-scale integration of artificial atoms in hybrid photonic circuits. *Nature* **583**, 226–231 (2020).
153. Santori, C. et al. Nanophotonics for quantum optics using nitrogen-vacancy centers in diamond. *Nanotechnology* **21**, 274008 (2010).
154. Alkahtani, M. H. et al. Fluorescent nanodiamonds: past, present, and future. *Nanophotonics* **7**, 1423–1453 (2018).
155. Radtke, M., Bernardi, E., Slablab, A., Nelz, R. & Neu, E. Nanoscale sensing based on nitrogen vacancy centers in single crystal diamond and nanodiamonds: achievements and challenges. *Nano Futures* **3**, 042004 (2019).
156. Barclay, P. E., Santori, C., Fu, K. M., Beausoleil, R. G. & Painter, O. Coherent interference effects in a nano-assembled diamond NV center cavity-QED system. *Opt. Express* **17**, 8081–8097 (2009).
157. Alagappan, G., Krivitsky, L. A. & Png, C. E. Diamond in a nanopocket: a new route to a strong purcell effect. *ACS Omega* **3**, 4733–4742 (2018).
158. Sahoo, S., Davydov, V. A., Agafonov, V. N., Bogdanov, S. I. Hybrid quantum nanophotonic devices with color centers in nanodiamonds [Invited]. *Opt. Mater. Express* **13**, 191–217 (2022).
159. Radulaski, M. et al. Nanodiamond integration with photonic devices. *Laser Photon. Rev.* **13**, 1800316 (2019).
160. Ngan, K., Zhan, Y., Dory, C., Vuckovic, J. & Sun, S. Quantum photonic circuits integrated with color centers in designer nanodiamonds. *Nano Lett.* **23**, 9360–9366 (2023).
161. Fehler, K. G. et al. Purcell-enhanced emission from individual SiV− center in nanodiamonds coupled to a Si3N4-based, photonic crystal cavity. *Nanophotonics* **9**, 3655–3662 (2020).
162. Antoniuk, L. et al. All-optical spin access via a cavity-broadened optical transition in on-chip hybrid quantum photonics. *Phys. Rev. Appl.* **21**, 054032 (2024).

163. Schrinner, P. P. J., Olthaus, J., Reiter, D. E. & Schuck, C. Integration of diamond-based quantum emitters with nanophotonic circuits. *Nano Lett.* **20**, 8170–8177 (2020).
164. Weng, H. C. et al. Heterogeneous integration of solid-state quantum systems with a foundry photonics platform. *ACS Photon.* **10**, 3302–3309 (2023).
165. Fu, K. M. C. et al. Coupling of nitrogen-vacancy centers in diamond to a GaP waveguide. *Appl. Phys. Lett.* **93**, 234107 (2008).
166. Barclay, P. E., Fu, K.-M. C., Santori, C., Faraon, A. & Beausoleil, R. G. Hybrid nanocavity resonant enhancement of color center emission in diamond. *Phys. Rev. X* **1**, 01007 (2011).
167. Gould, M. et al. Large-scale GaP-on-diamond integrated photonics platform for NV center-based quantum information. *J. Opt. Soc. Am. B* **33**, B35–B42 (2016).
168. Wilson, D. J. et al. Integrated gallium phosphide nonlinear photonics. *Nat. Photon.* **14**, 57–62 (2019).
169. Zadeh, I. E. et al. Deterministic integration of single photon sources in silicon based photonic circuits. *Nano Lett.* **16**, 2289–2294 (2016).
170. Elshaari, A. W. et al. On-chip single photon filtering and multiplexing in hybrid quantum photonic circuits. *Nat. Commun.* **8**, 379 (2017).
171. Kim, J. H. et al. Hybrid integration of solid-state quantum emitters on a silicon photonic chip. *Nano Lett.* **17**, 7394–7400 (2017).
172. Chanana, A. et al. Ultra-low loss quantum photonic circuits integrated with single quantum emitters. *Nat. Commun.* **13**, 7693 (2022).
173. Katsumi, R., Ota, Y., Kakuda, M., Iwamoto, S. & Arakawa, Y. Transfer-printed single-photon sources coupled to wire waveguides. *Optica* **5**, 691 (2018).
174. Katsumi, R. et al. Quantum-dot single-photon source on a CMOS silicon photonic chip integrated using transfer printing. *APL Photon.* **4**, 036105 (2019).
175. Pholsen, N. et al. Nanocavity-based quantum-dot single-photon source on a SiN waveguide integrated by transfer printing. *Opt. Express* **33**, 252–262 (2025).
176. Katsumi, R. et al. CMOS-compatible integration of telecom band InAs/InP quantum-dot single-photon sources on a Si chip using transfer printing. *Appl. Phys. Express* **16**, 012004 (2022).
177. Davanco, M. et al. Heterogeneous integration for on-chip quantum photonic circuits with single quantum dot devices. *Nat. Commun.* **8**, 889 (2017).
178. Schnauber, P. et al. Indistinguishable photons from deterministically integrated single quantum dots in heterogeneous GaAs/Si(3)N(4) quantum photonic circuits. *Nano Lett.* **19**, 7164–7172 (2019).
179. Ellis, D. J. P. et al. Independent indistinguishable quantum light sources on a reconfigurable photonic integrated circuit. *Appl. Phys. Lett.* **112**, 211104 (2018).
180. Peyskens, F., Chakraborty, C., Muneeb, M., Van Thourhout, D. & Englund, D. Integration of single photon emitters in 2D layered materials with a silicon nitride photonic chip. *Nat. Commun.* **10**, 4435 (2019).
181. Parto, K. et al. Cavity-Enhanced 2D material quantum emitters deterministically integrated with silicon nitride microresonators. *Nano Lett.* **22**, 9748–9756 (2022).
182. Chakraborty, U. et al. Cryogenic operation of silicon photonic modulators based on the DC Kerr effect. *Optica* **7**, 1385 (2020).
183. Dong, M. et al. High-speed programmable photonic circuits in a cryogenically compatible, visible–near-infrared 200 mm CMOS architecture. *Nat. Photon* **16**, 59–65 (2021).
184. Xue, X. et al. CMOS-based cryogenic control of silicon quantum circuits. *Nature* **593**, 205–210 (2021).
185. Ruffino, A. et al. A cryo-CMOS chip that integrates silicon quantum dots and multiplexed dispersive readout electronics. *Nat. Electron* **5**, 53–59 (2021).
186. Pauka, S. J. et al. A cryogenic CMOS chip for generating control signals for multiple qubits. *Nat. Electron* **4**, 64–70 (2021).
187. Hornibrook, J. M. et al. Cryogenic control architecture for large-scale quantum computing. *Phys. Rev. Appl.* **3**, 024010 (2015).
188. Gambetta, J. M., Chow, J. M. & Steffen, M. Building logical qubits in a superconducting quantum computing system. *npj Quantum Inform.* **3**, 2 (2017).
189. Bao, Z. et al. A cryogenic on-chip microwave pulse generator for large-scale superconducting quantum computing. *Nat. Commun.* **15**, 5958 (2024).
190. Li, L. et al. Heterogeneous integration of spin-photon interfaces with a CMOS platform. *Nature* **630**, 70–76 (2024).
191. Lee, J., Karnadi, I., Kim, J. T., Lee, Y.-H. & Kim, M.-K. Printed Nanolaser on Silicon. *ACS Photon.* **4**, 2117–2123 (2017).
192. Zhang, J. et al. III-V-on-Si photonic integrated circuits realized using micro-transfer-printing. *APL Photon.* **4**, 110803 (2019).
193. Smith, J. A., Jevtics, D., Guilhabert, B., Dawson, M. D. & Strain, M. J. Hybrid integration of chipscale photonic devices using accurate transfer printing methods. *Appl. Phys. Rev.* **9**, 041317 (2022).
194. Katsumi, R. et al. Transfer-printing-based integration of silicon nitride grating structure on single-crystal diamond toward sensitive magnetometers. *Appl Phys. Lett.* **121**, 161103 (2022).
195. Khanaliloo, B. et al. Single-Crystal diamond nanobeam waveguide optomechanics. *Phys. Rev. X* **5**, 041051 (2015).
196. Katsumi, R. et al. High-sensitivity nanoscale quantum sensors based on a diamond micro-resonator. *Commun. Mater*. **6**, 49 (2025).
197. Kim, D. et al. A CMOS-integrated quantum sensor based on nitrogen–vacancy centres. *Nat. Electron* **2**, 284–289 (2019).
198. Webb, J. L. et al. Nanotesla sensitivity magnetic field sensing using a compact diamond nitrogen-vacancy magnetometer. *Appl. Phys. Lett.* **114**, 231103 (2019).
199. Patel, R. L. et al. Subnanotesla Magnetometry with a Fiber-Coupled Diamond Sensor. *Phys. Rev. Appl.* **14**, 044058 (2020).
200. Kuwahata, A. et al. Magnetometer with nitrogen-vacancy center in a bulk diamond for detecting magnetic nanoparticles in biomedical applications. *Sci. Rep.* **10**, 2483 (2020).
201. Stürner, F. M. et al. Integrated and portable magnetometer based on nitrogen-vacancy ensembles in. *Diam. Adv. Quantum Technol.* **4**, 2000111 (2021).
202. Kainuma, Y. et al. Compact and stable diamond quantum sensors for wide applications. *Adv. Quantum Technol.* **7**, 2300456 (2024).
203. Deguchi, H. et al. Compact and portable quantum sensor module using diamond NV centers. *Appl. Phys. Express* **16**, 062004 (2023).
204. Ruf, M. et al. Optically coherent nitrogen-vacancy centers in micrometer-thin etched diamond membranes. *Nano Lett.* **19**, 3987–3992 (2019).
205. Kumar, R. et al. Stability of near-surface nitrogen vacancy centers using dielectric surface passivation. *ACS Photon.* **11**, 1244–1251 (2024).
206. Kaviani, M. et al. Proper surface termination for luminescent near-surface NV centers in diamond. *Nano Lett.* **14**, 4772–4777 (2014).
207. Geng, J. et al. Dopant-assisted stabilization of negatively charged single nitrogen-vacancy centers in phosphorus-doped diamond at low temperatures. *npj Quantum Inform.* **9**, 110 (2023).
208. Haruyama, M. et al. Charge stabilization of shallow nitrogen-vacancy centers using graphene/diamond junctions. *Appl. Phys. Lett.* **122**, 141601 (2023).
209. Machielse, B. et al. Quantum interference of electromechanically stabilized emitters in nanophotonic devices. *Phys. Rev. X* **9**, 031022 (2019).
210. McPhillimy, J. et al. Automated nanoscale absolute accuracy alignment system for transfer printing. *ACS Appl. Nano Mater.* **3**, 10326–10332 (2020).
211. Zhang, J. et al. III-V-on-Si photonic integrated circuits realized using micro-transfer-printing. *Apl. Photon.* **4**, 110803 (2019).

212. Makino, T. et al. Diamond Schottky-pn diode with high forward current density and fast switching operation. *Appl. Phys. Lett.* **94**, 262101 (2009).
213. Tonndorf, P. et al. On-Chip waveguide coupling of a layered semiconductor single-photon source. *Nano Lett.* **17**, 5446–5451 (2017).
214. Huber, T. et al. Filter-free single-photon quantum dot resonance fluorescence in an integrated cavity-waveguide device. *Optica* **7**, 380–385 (2020).
215. Uppu, R. et al. On-chip deterministic operation of quantum dots in dual-mode waveguides for a plug-and-play single-photon source. *Nat. Commun.* **11**, 3782 (2020).
216. Patel, R. N. et al. Efficient photon coupling from a diamond nitrogen vacancy center by integration with silica fiber. *Light Sci. Appl.* **5**, e16032 (2016).
217. Zeng, B. et al. Cryogenic packaging of nanophotonic devices with a low coupling loss <1 dB. *Appl. Phys. Lett.* **123**, 161106 (2023).
218. Parker, R. A. et al. A diamond nanophotonic interface with an optically accessible deterministic electronuclear spin register. *Nat. Photon*. **18**, 156–161 (2023).
219. Grotz, B. et al. Charge state manipulation of qubits in diamond. *Nat. Commun.* **3**, 729 (2012).
220. Aslam, N., Waldherr, G., Neumann, P., Jelezko, F. & Wrachtrup, J. Photo-induced ionization dynamics of the nitrogen vacancy defect in diamond investigated by single-shot charge state detection. *N. J. Phys.* **15**, 013064 (2013).
221. Doi Y. et al. Deterministic electrical charge-state initialization of single nitrogen-vacancy center in diamond. *Phys. Rev. X* **4**, 011057 (2014).
222. Doi, Y. et al. Pure negatively charged state of the NV center inn-type diamond. *Phys. Rev. B* **93**, 081203 (2016).
223. Dhomkar, S., Zangara, P. R., Henshaw, J. & Meriles, C. A. On-demand generation of neutral and negatively charged silicon-vacancy centers in diamond. *Phys. Rev. Lett.* **120**, 117401 (2018).
224. Shinei, C. et al. Equilibrium charge state of NV centers in diamond. *Appl. Phys. Lett.* **119**, 254001 (2021).
225. Lozovoi, A. et al. Optical activation and detection of charge transport between individual colour centres in diamond. *Nat. Electron* **4**, 717–724 (2021).
226. Pederson, C. et al. Rapid, in Situ neutralization of nitrogen- and silicon-vacancy centers in diamond using above-band gap optical excitation. *Nano Lett.* **25**, 673–680 (2025).
227. Volker, L. A. et al. Charge and spin dynamics and destabilization of shallow nitrogen-vacancy centers under UV and blue excitation. *Nano Lett.* **24**, 11895–11903 (2024).
228. Bernien, H. et al. Two-photon quantum interference from separate nitrogen vacancy centers in diamond. *Phys. Rev. Lett.* **108**, 043604 (2012).
229. Golter, D. A., Oo, T., Amezcua, M., Stewart, K. A. & Wang, H. Optomechanical quantum control of a nitrogen-vacancy center in diamond. *Phys. Rev. Lett.* **116**, 143602 (2016).
230. Tamarat, P. et al. Stark shift control of single optical centers in diamond. *Phys. Rev. Lett.* **97**, 083002 (2006).
231. Meesala, S. et al. Strain engineering of the silicon-vacancy center in diamond. *Phys. Rev. B* **97**, 205444 (2018).
232. De Santis, L., Trusheim, M. E., Chen, K. C. & Englund, D. R. Investigation of the Stark Effect on a centrosymmetric quantum emitter in diamond. *Phys. Rev. Lett.* **127**, 147402 (2021).
233. Ryan, C. A., Hodges, J. S. & Cory, D. G. Robust decoupling techniques to extend quantum coherence in diamond. *Phys. Rev. Lett.* **105**, 200402 (2010).
234. de Lange, G., Wang, Z. H., Riste, D., Dobrovitski, V. V. & Hanson, R. Universal dynamical decoupling of a single solid-state spin from a spin bath. *Science* **330**, 60–63 (2010).
235. Naydenov, B. et al. Dynamical decoupling of a single-electron spin at room temperature. *Phys. Rev. B* **83**, 081201 (2011).
236. Pham, L. M. et al. Enhanced solid-state multispin metrology using dynamical decoupling. *Phys. Rev. B* **86**, 045214 (2012).
237. Brandenburg, F. et al. Improving the electron spin properties of nitrogen-vacancy centres in nanodiamonds by near-field etching. *Sci. Rep.* **8**, 15847 (2018).
238. Sangtawesin, S. et al. Origins of diamond surface noise probed by correlating single-spin measurements with surface spectroscopy. *Phys. Rev. X* **9**, 031052 (2019).
239. Herbschleb, E. D. et al. Ultra-long coherence times amongst room-temperature solid-state spins. *Nat. Commun.* **10**, 3766 (2019).
240. Tsukamoto, M. et al. Vector magnetometry using perfectly aligned nitrogen-vacancy center ensemble in diamond. *Appl Phys. Lett.* **118**, 264002 (2021).
241. Kajiyama, K. et al. Heteroepitaxial (111) diamond quantum sensors with preferentially aligned nitrogen-vacancy centers for an electric vehicle battery monitor. *Adv. Quantum Technol.* **8**, 2400400 (2025).
242. Jeske, J., Cole, J. H. & Greentree, A. D. Laser threshold magnetometry. *N. J. Phys.* **18**, 013015 (2016).
243. Jeske, J. et al. Stimulated emission from nitrogen-vacancy centres in diamond. *Nat. Commun.* **8**, 14000 (2017).
244. Raman Nair, S. et al. Amplification by stimulated emission of nitrogen-vacancy centres in a diamond-loaded fibre cavity. *Nanophotonics* **9**, 4505–4518 (2020).
245. Hahl, F. et al. Magnetic-Field-Dependent stimulated emission from nitrogen-vacancy centres in diamond. **8**, eabn7192 (2022).
246. Su, C. et al. Fundamentals and emerging optical applications of hexagonal boron nitride: a tutorial. *Adv. Opt. Photon.* **16**, 229–346 (2024).
247. Gottscholl, A. et al. Initialization and read-out of intrinsic spin defects in a van der Waals crystal at room temperature. *Nat. Mater.* **19**, 540–545 (2020).
248. Katsumi, R., Sekino, M. & Yatsui, T. Design of an ultra-sensitive and miniaturized diamond NV magnetometer based on a nanocavity structure. *Jpn J. Appl Phys.* **61**, 082004 (2022).
249. Solntsev, A. S., Agarwal, G. S. & Kivshar, Y. S. Metasurfaces for quantum photonics. *Nat. Photon.* **15**, 327–336 (2021).
250. Neshev, D. N. & Miroshnichenko, A. E. Enabling smart vision with metasurfaces. *Nat. Photon.* **17**, 26–35 (2022).
251. Monticone, F. & Alu, A. Metamaterial, plasmonic and nanophotonic devices. *Rep. Prog. Phys.* **80**, 036401 (2017).
252. Hatano, Y. et al. High-precision robust monitoring of charge/discharge current over a wide dynamic range for electric vehicle batteries using diamond quantum sensors. *Sci. Rep.* **12**, 13991 (2022).
253. Fujiwara, M. Diamond quantum sensors in microfluidics technology. *Biomicrofluidics* **17**, 054107 (2023).
254. Ebadi, R. et al. Directional detection of dark matter using solid-state quantum sensing. *AVS Quantum Sci.* **4**, 044701 (2022).
255. Clarke, J. & Alex I, B. *The SQUID handbook: Applications of SQUIDs and SQUID systems (Wiley & Sons*, 2006).
256. Shah, V. K. & Wakai, R. T. A compact, high performance atomic magnetometer for biomedical applications. *Phys. Med Biol.* **58**, 8153–8161 (2013).

Acknowledgements

We acknowledge funding from the MEXT Quantum Leap Flagship Program (MEXT Q-LEAP, Grant Number JPMXS0118067395), PRESTO (Grant Numbers JPMJPR24F1) and KAKENHI (Grant Numbers 21K20428, 23K22795, 22K14289, and 23KK0268), as well as Asahi Glass Foundation, Marubun Foundation, Hibi Science Foundation, Nippon Sheet Glass Foundation for Materials Science and Engineering, and Murata Foundation.

Author contributions
R.K. and K.T. researched data for the article. All authors contributed substantially to discussion of the content. All authors wrote the article. All authors reviewed and/or edited the manuscript before submission.

Competing interests
The authors declare no competing interests.

Additional information
Supplementary information The online version contains supplementary material available at https://doi.org/10.1038/s44172-025-00398-2.

Correspondence and requests for materials should be addressed to Ryota Katsumi.

Peer review information *Communications Engineering* thanks Minghao Li and the other, anonymous, reviewers for their contribution to the peer review of this work. Primary Handling Editors: [Anastasiia Vasylchenkova, Miranda Vinay and Rosamund Daw]. Peer review reports are available.

Reprints and permissions information is available at http://www.nature.com/reprints

Publisher's note Springer Nature remains neutral with regard to jurisdictional claims in published maps and institutional affiliations.